



HAL
open science

Harmonic response of soil radon-222 flux and concentration induced by barometric oscillations

Frédéric Perrier, Frédéric Girault

► **To cite this version:**

Frédéric Perrier, Frédéric Girault. Harmonic response of soil radon-222 flux and concentration induced by barometric oscillations. *Geophysical Journal International*, 2012, 195 (2), pp.945-971. 10.1093/gji/ggt280 . insu-01298238

HAL Id: insu-01298238

<https://insu.hal.science/insu-01298238>

Submitted on 5 Apr 2016

HAL is a multi-disciplinary open access archive for the deposit and dissemination of scientific research documents, whether they are published or not. The documents may come from teaching and research institutions in France or abroad, or from public or private research centers.

L'archive ouverte pluridisciplinaire **HAL**, est destinée au dépôt et à la diffusion de documents scientifiques de niveau recherche, publiés ou non, émanant des établissements d'enseignement et de recherche français ou étrangers, des laboratoires publics ou privés.

Harmonic response of soil radon-222 flux and concentration induced by barometric oscillations

Frédéric Perrier and Frédéric Girault

Equipe de Géomagnétisme, Institut de Physique du Globe de Paris, Sorbonne Paris Cité, Université Paris Diderot, UMR 7154 CNRS, 1 rue Jussieu, F-75005 Paris, France. E-mail: perrier@ipgp.fr

Accepted 2013 July 15. Received 2013 July 1; in original form 2012 September 26

SUMMARY

Radon-222 flux and concentration in the soil are sensitive to changes in atmospheric pressure, and in particular to periodic signals, such as the semi-diurnal barometric tide S2. The response of radon flux and concentration to barometric oscillations is calculated analytically for all harmonic degrees in the case of a horizontal layer over a half-space, representing the situation of a soil layer over homogeneous bedrock, taking into account air and water phases and the presence of static vertical advection. The calculations show that the presence of an interface changes dramatically the response to barometric oscillations. Large amplitudes at the forcing frequency (fundamental) are concentrated in the vicinity of the interface, while amplitudes remain negligible at the same depth in a homogeneous half-space. A significant negative phase shift in the surface radon flux is introduced when a shallow interface is present, while radon flux is almost in phase opposition with atmospheric pressure over a homogeneous half-space. While, in most situations, the amplitudes are small and difficult to detect, situations can be exhibited where the amplitudes of harmonics 2 and 3 of radon concentration are larger than 100 Bq m^{-3} , leading, for example, to possible detection of 4-hr peaks in the radon power spectra due to barometric tide S2. Optimal position of the radon sensors appears to be a few centimetres in the bedrock below the soil. Amplitudes of radon concentration and surface flux are sensitive to underlying bedrock permeability, porosity, water saturation and effective radium concentration, and depend also on the presence of advection. At large carrier gas velocities, a more precise calculation valid for multilayered media, is presented, which can be used in volcanic and hydrothermal areas. While the amplitudes of all harmonics for radon concentration in the soil become negligible, the fundamental in radon surface flux reaches a constant and, possibly, observable value dominated by the parameters of the deepest medium. A better knowledge of the response of radon flux and concentration to barometric oscillations is important to interpret the presence or absence of peaks in the power spectra of radon time-series collected for environmental and geodynamical purposes. This study provides further support to the relevance of long-term radon monitoring to constrain the transport properties of the subsurface.

Key words: Non-linear differential equations; Gas and hydrate systems; Hydrothermal systems; Permeability and porosity; Fracture and flow.

1 INTRODUCTION

Radon-222 is a noble gas, decay product of radium-226 in the uranium-238 decay chain, and itself radioactive with half-life of 3.8 d. It is released from minerals and groundwater into the pore space of rocks and soils, and subsequently transported to the ground surface by diffusive or advective processes (Tanner 1964; Nazaroff 1992). While radon-222 is important to study because it represents more than half of the radiation dose to the general population (Porstendörfer 1994), and thus constitutes a major cause of lung cancer, second only to smoking (Darby *et al.* 2004; Al-Zoughool & Krewski 2009), it is also a valuable tool to study shallow or deep subsurface processes in the context of environmental or geodynamical problems (Tanner 1964; Gillmore *et al.* 2010). In fact, thanks to the availability of robust and cost-effective sensors (Papastefanou 2002), radon-222 concentration in the soil is being studied extensively on volcanoes (Eff-Darwich *et al.* 2002; Neri *et al.* 2006; Laiolo *et al.* 2012) and tectonic active zones (Baykara *et al.* 2005; Richon *et al.* 2007; Steinitz & Piatibratova 2010; Choubey *et al.* 2011; Kamra *et al.* 2013; Zafir *et al.* 2013).

In order to derive geodynamically relevant information from radon time-series, it is important, however, that other effects, such as instrumental artefacts or meteorological forcing, are understood and modelled sufficiently well. Radon concentration in the soil is affected primarily by precipitation (Kitto 2005; Perrier *et al.* 2009a), but also soil temperature (Washington & Rose 1992), wind speed (Holford *et al.* 1993; Riley *et al.* 1996, 1999) and atmospheric pressure (Clements & Wilkening 1974; Schery & Gaeddert 1982; Robinson *et al.* 1997). The effect of atmospheric pressure variations was first recognized in temperature-stable underground settings (Pohl-Rüling & Pohl 1969), where it has a relatively simple signature, with radon concentration increase associated with pressure deficit, due to pumping of radon-rich pore air into the atmosphere. This barometric pumping effect, which can be spectacular, for example, in the access zone of underground cavities (Perrier *et al.* 2004), is now reasonably well understood and modelled (Viñas *et al.* 2007; Perrier & Richon 2010). In the soil, the relationship between radon concentration and atmospheric pressure is more difficult to observe because of the interplay with other effects, such as temperature (Sundal *et al.* 2008) or water infiltration (Perrier *et al.* 2009a). When pressure sensitivity is observed, radon concentration in the soil is usually decreasing during pressure drops, but the relationship between radon and pressure can be difficult to identify and, in addition, can be time-dependent (Schery *et al.* 1984; Owczarski *et al.* 1990; Holford *et al.* 1993; Fujiyoshi *et al.* 2006).

To study the effect of atmospheric pressure variations in the soil, one can use transient, large meteorological perturbations, such as mid-latitude cyclones (Perrier & Richon 2010) or typhoons (Richon *et al.* 2003). Such transient signals are particularly important to study when searching for transient radon signals associated with earthquakes (Richon *et al.* 2003; Crockett *et al.* 2006) or volcanic eruptions (Cigolini *et al.* 2009). Another tool is provided by the barometric tides, such as the diurnal variation S1, and, almost systematically larger than S1, the semi-diurnal oscillation S2. One method to identify atmospheric pressure sensitivity of radon signals, therefore, is to examine the presence of S2 peak in the power spectra of time-series (Barbosa *et al.* 2007, 2010; Steinitz *et al.* 2007; Richon *et al.* 2009; Crockett *et al.* 2010; Steinitz & Piatibratova 2010; Zafirir *et al.* 2013). The response to barometric tide actually provides a relevant *in situ* method to characterize the transport properties of the soil (Massmann & Farrier 1992; Pinault & Baubron 1996; Neeper 2002) and to monitor these properties as a function of time (Richon *et al.* 2011). Radon response in this case also offers a powerful proxy for contaminant transport in the shallow subsurface (Nilson *et al.* 1991; Auer *et al.* 1996). Recent theoretical developments, thus, focused on contaminant transport (Neeper & Stauffer 2005). Detailed calculations of the effect of barometric oscillations have now also been presented in the case of CO₂ (Massman 2006), which paved the way to develop similar interpretation tools for radon.

In this paper, we present an analytical calculation of the response of radon flux and concentration to barometric oscillations for all harmonic degrees in the case of a horizontal layer over a half-space, representing the simplified situation of a soil layer over homogeneous bedrock, taking into account air and water phases and the presence of static vertical pore gas advection. Selected results of these calculations are presented together with sensitivity studies, as well as the particular case of advection-dominated transport, a limiting case useful for volcanic and degassing hydrothermal areas.

2 CALCULATION OF THE HARMONIC RESPONSE IN THE PRESENCE OF SLIGHT ADVECTION

2.1 Assumptions and model parameters

Consider a homogeneous porous medium indexed 1 above a homogeneous half-space indexed 2, with vertical axis z oriented upwards with ground surface at $z = 0$ and the horizontal interface between the two media located at $z = z_1 < 0$. In the following, medium 1 is sometimes referred to simply as the ‘soil’ layer, and medium 2 as the ‘bedrock’. This idealized situation is actually more general, and might also apply to other situations, for example, one layer of permeable soil over soaked sediments, or one homogeneous unsaturated sand layer over a thick soaked sandy layer, or alternatively, one layer of poorly permeable clayey soil over a thick permeable sand deposit.

Each medium j is characterized by permeability k_j , porosity ε_j , volumetric water saturation S_{wj} and mineral matrix density ρ_j . The radon source term in medium j is the effective radium concentration EC_{Raj} (Stoulos *et al.* 2003), product of the radium-226 activity concentration C_{Ra} and the emanation factor E (Tanner 1964; Sakoda *et al.* 2011). In the outside atmosphere ($z > 0$), radon concentration is assumed to remain homogeneous and constant with time, with concentration c_e . This is valid for timescales and frequency scales allowing a well-mixed boundary layer.

In addition, we allow the possibility of a vertical constant gas flow, characterized by a specific (volumetric) flow rate V_0 per unit area (Darcy velocity). This situation occurs, for example, in volcanic and hydrothermal areas (Viveiros *et al.* 2008, 2010; Perrier *et al.* 2009b; Laiolo *et al.* 2012; Kämpf *et al.* 2013), and can possibly occur in the case of leakage from a natural or artificial CO₂ reservoir (Lewicki *et al.* 2007).

Let us now consider a stationary oscillation of surface atmospheric pressure with frequency f and amplitude p_0 . Excess surface pressure p_s accordingly is written $p_s(t) = p_0 e^{i\omega t}$, where t is time and $\omega = 2\pi f$. Our goal is to compute the response for radon concentration everywhere in the subsurface $c(z, t)$ and the resulting radon flux $\Phi_s(t)$ at the surface.

In response to the surface forcing, excess pressure in pore gas $p(z, t)$ is assumed to obey a diffusion equation (Nilson *et al.* 1991; Holford *et al.* 1993):

$$\frac{\partial p}{\partial t} = \alpha_p \frac{\partial^2 p}{\partial z^2}, \quad (1)$$

where α_j is the pneumatic diffusivity in medium j , given by:

$$\alpha_j = \frac{k_j^g P_0}{\varepsilon_j^g \eta_g}. \quad (2)$$

In eq. (2), P_0 is the average atmospheric pressure (1010 hPa when not stated otherwise), k_j^g the gas phase permeability in medium j , ε_j^g the pore gas porosity, equal to $\varepsilon_j(1 - S_{wj})$ and η_g the dynamic viscosity of air (1.8×10^{-5} Pa s). The gas phase permeability is written $k_j^g = k_j k_r(S_{wj})$, taking for the relative air permeability $k_r(S_{wj})$ the simplified expression $k_r(S_w) = (1 - S_{\text{eff}})^2 / (1 - S_{\text{eff}}^2)$ with $S_{\text{eff}} = (S_w - S_w^0) / (1 - S_w^0)$ and $S_w^0 = 0.01$. In this work, all pressure variations are assumed to be small compared with P_0 .

In each medium, the spatial and temporal variations of radon concentration in pore air $c(z, t)$ are given by the following equation (Rogers & Nielson 1991b; Nazaroff 1992; Holford *et al.* 1993; Lehmann *et al.* 2000; Ho 2008):

$$\frac{\partial c_j}{\partial t} = D_j \frac{\partial^2 c}{\partial z^2} - W_j \frac{\partial c_j}{\partial z} + \lambda (\hat{c}_j - c_j), \quad (3)$$

where D_j is the effective radon diffusion coefficient, W_j the effective advection parameter, λ the radon-222 decay constant (2.1×10^{-6} s $^{-1}$) and \hat{c}_j the source term, equal to the radon concentration at radioactive equilibrium in the absence of transport. Neglecting diffusion effects in water, motion of water and adsorption, we have (Nazaroff 1992; Lehmann *et al.* 2000):

$$\left\{ \begin{array}{l} D_j = \frac{\varepsilon_j^g D_j^g}{\varepsilon_j^g + \varepsilon_j^w \kappa_w} \\ W_j = \frac{F_j}{\varepsilon_j^g + \varepsilon_j^w \kappa_w} \\ \hat{c}_j = \frac{EC_{\text{Ra}j}(S_{wj})\rho_j(1 - S_{wj})}{\varepsilon_j^g + \varepsilon_j^w \kappa_w} \end{array} \right., \quad (4)$$

where $F_j(z, t)$ is the specific gas flow rate, $\kappa_w(T) = 0.104 + 0.416e^{-0.0491T}$ (Girault & Perrier 2012a) the partition coefficient of radon between water and air, function of the mean temperature T , expressed in $^{\circ}\text{C}$, ε_j^w the water-filled porosity, equal to $\varepsilon_j S_{wj}$ and D_j^g the diffusion coefficient of radon in the considered porous medium. In this paper, we use the empirical relation (Rogers & Nielson 1991a) $D^g(\varepsilon, S_w) = D_0 \varepsilon e^{-6\varepsilon S_w - 6.514\varepsilon^2}$, where D_0 is the diffusion coefficient of radon in air (1.2×10^{-5} m 2 s $^{-1}$). Dispersion and anisotropy effects (Massman 2006) are not considered here. In the following, we also define $W_{j0} = V_0 / (\varepsilon_j^g + \varepsilon_j^w \kappa_w)$. To take into account the slight variation of EC_{Ra} with saturation S_w (Sakoda *et al.* 2011), the set value of EC_{Ra} is multiplied by the empirical function $32.89e^{-2.120S_w} - 32.02e^{-2.225S_w}$ for soil and $31.55e^{-1.635S_w} - 30.83e^{-1.733S_w}$ for bedrock (Girault & Perrier 2012b).

The specific flow rate $F_j(z, t)$ is expressed as:

$$F_j = V_0 - \frac{k_j^g}{\eta_g} \frac{\partial p_j}{\partial z}, \quad (5)$$

and the radon flux $\Phi_j(z, t)$ as (Nazaroff 1992):

$$\Phi_j = F_j c_j - \varepsilon_j^g D_j^g \frac{\partial c_j}{\partial z}. \quad (6)$$

2.2 Pore airflow response to barometric oscillations

In the case of our two-medium configuration, the solution for pressure variations in each medium reads (Nilson *et al.* 1991; Perrier & Richon 2010):

$$p_j(z, t) = p_0 e^{i\omega t} (A_j e^{\gamma_j(1+i)z} + B_j e^{-\gamma_j(1+i)z}), \quad (7)$$

where A_j and B_j are constants and γ_j (inverse of the pneumatic attenuation length) is:

$$\gamma_j = \sqrt{\frac{\omega}{2\alpha_j}}. \quad (8)$$

A finite solution for $z = -\infty$ imposes $B_2 = 0$ while the boundary condition $p_1(z = 0, t) = p_s(t)$ imposes $A_1 + B_1 = 1$. Continuity of pressure and conservation of the flow at $z = z_1$ then gives two additional conditions:

$$\begin{cases} A_1 a_1 + B_1 b_1 = A_2 a_2 \\ A_1 a_1 - B_1 b_1 = r A_2 a_2 \end{cases}, \quad (9)$$

where

$$a_j = e^{\gamma_j(1+i)z_1}, \quad b_j = e^{-\gamma_j(1+i)z_1} = a_j^{-1}, \quad (10)$$

and

$$r = \frac{k_2^g \gamma_2}{k_1^g \gamma_1} = \frac{k_2^g}{k_1^g} \sqrt{\frac{\alpha_1}{\alpha_2}} = \sqrt{\frac{k_2^g \varepsilon_2^g}{k_1^g \varepsilon_1^g}}. \tag{11}$$

The solution for the constants is then given by:

$$\begin{cases} A_1 = \frac{b_1(1+r)}{a_1(1-r) + b_1(1+r)} \\ B_1 = \frac{a_1(1-r)}{a_1(1-r) + b_1(1+r)} \\ A_2 = \frac{2}{a_2(a_1(1-r) + b_1(1+r))} \end{cases}. \tag{12}$$

Using eq. (5), the solution for the specific flow rate is:

$$F_j = V_0 - \frac{k_j^g}{\eta} \frac{\partial p_j}{\partial z} = V_0 - \frac{k_j^g}{\eta} \gamma_j (1+i) p_0 e^{i\omega t} (A_j e^{\gamma_j(1+i)z} - B_j e^{-\gamma_j(1+i)z}), \tag{13}$$

which we write, for later convenience:

$$F_j = V_0 - s_j \varepsilon_j^g e^{i\omega t} (1+i) (A_j e^{\gamma_j(1+i)z} - B_j e^{-\gamma_j(1+i)z}), \tag{14}$$

defining the frequency dependent parameter:

$$s_j = \frac{k_j^g \gamma_j}{\eta \varepsilon_j^g} p_0. \tag{15}$$

2.3 Radon flux and concentration response to barometric oscillations

2.3.1 General harmonic expansion

To find a solution of the non-linear differential equation eq. (3), we follow the linearization method used by Massman (2006) and we write the solution as a harmonic expansion:

$$c_j(z, t) = c_{j0}(z) + \sum_{n=1}^{\infty} c_{jn}(z) e^{in\omega t} e^{n\gamma_j(1+i)z}. \tag{16}$$

The expansion eq. (16) introduces the functions $c_{jn}(z)$, which are the harmonic n terms of the radon concentration in layer j . In this expansion, the term $n = 0$ is the static solution, $n = 1$ the response at the forcing frequency (fundamental frequency) and the terms $n \geq 2$ correspond to the higher harmonics resulting from the non-linear coupling between the radon evolution equation and the gas flow. In the limit of large atmospheric mixing compared with the characteristic transport times of radon, we have $c_{1n}(z = 0) = 0$ for $n \geq 1$.

Using eq. (16), we can write the harmonic expansion of the derivatives:

$$\begin{cases} \frac{\partial c_j}{\partial t} = \sum_{n=1}^{\infty} c_{jn} i n \omega e^{in\omega t} e^{n\gamma_j(1+i)z} \\ \frac{\partial c_j}{\partial z} = \frac{dc_{j0}}{dz} + \sum_{n=1}^{\infty} \left(\frac{dc_{jn}}{dz} + n\gamma_j(1+i)c_{jn} \right) e^{in\omega t} e^{n\gamma_j(1+i)z} \\ \frac{\partial^2 c_j}{\partial z^2} = \frac{d^2 c_{j0}}{dz^2} + \sum_{n=1}^{\infty} \left(\frac{d^2 c_{jn}}{dz^2} + 2n\gamma_j(1+i) \frac{dc_{jn}}{dz} + 2in^2 \gamma_j^2 c_{jn} \right) e^{in\omega t} e^{n\gamma_j(1+i)z} \end{cases}, \tag{17}$$

and of the surface radon flux $\Phi_s(t)$:

$$\Phi_s(t) = \Phi_1(0, t) = F_1 c_e - \varepsilon_1^g D_1^g \frac{\partial c_1}{\partial z} = \sum_{n=0}^{\infty} \Phi_{sn} e^{in\omega t}, \tag{18}$$

with

$$\begin{cases} \Phi_{s0} = V_0 c_e - \varepsilon_1^g D_1^g \left. \frac{dc_{10}}{dz} \right|_{z=0} \\ \Phi_{s1} = -s_1 \varepsilon_1^g c_e (1+i) (A_1 - B_1) - \varepsilon_1^g D_1^g \left. \frac{dc_{11}}{dz} \right|_{z=0} \\ \Phi_{sn \geq 2} = -\varepsilon_1^g D_1^g \left. \frac{dc_{1n}}{dz} \right|_{z=0} \end{cases}. \tag{19}$$

Injecting the expression of the derivatives eq. (17) into eq. (3), we obtain:

$$\begin{aligned} \sum_{n=1}^{\infty} c_{jn} i n \omega e^{i n \omega t} e^{n \gamma_j (1+i) z} &= \lambda \hat{c}_j - \lambda \left(c_{j0} + \sum_{n=1}^{\infty} c_{jn} e^{i n \omega t} e^{n \gamma_j (1+i) z} \right) - (W_{j0} - s_j (1+i) e^{i \omega t} (A_j e^{\gamma_j (1+i) z} - B_j e^{-\gamma_j (1+i) z})) \\ &\times \left(\frac{dc_{j0}}{dz} + \sum_{n=1}^{\infty} \left(\frac{dc_{jn}}{dz} + n \gamma_j (1+i) c_{jn} \right) e^{i n \omega t} e^{n \gamma_j (1+i) z} \right) \\ &+ D_j \left(\frac{d^2 c_{j0}}{dz^2} + \sum_{n=1}^{\infty} \left(\frac{d^2 c_{jn}}{dz^2} + 2n \gamma_j (1+i) \frac{dc_{jn}}{dz} + 2i n^2 \gamma_j^2 c_{jn} \right) e^{i n \omega t} e^{n \gamma_j (1+i) z} \right) \end{aligned} \quad (20)$$

The solutions for the harmonic functions $c_{jn}(z)$ can now be found from eq. (20) by identifying the harmonic terms in sequence (Massman 2006).

2.3.2 Static solution for radon concentration and flux

First, identifying the static terms with $n = 0$, we obtain the following equation for $c_{j0}(z)$:

$$D_j \frac{d^2 c_{j0}}{dz^2} - W_{j0} \frac{dc_{j0}}{dz} - \lambda c_{j0} = -\lambda \hat{c}_j. \quad (21)$$

This equation has a particular solution $c_{j0} = \hat{c}_j$ and the left-hand side has general solutions of the form $c_{j0}(z) = e^{\beta_{j0} z}$ with:

$$D_j \beta_{j0}^2 - W_{j0} \beta_{j0} - \lambda = 0, \quad (22)$$

thus:

$$\beta_{j0}^{\pm} = \frac{W_{j0} \pm \sqrt{W_{j0}^2 + 4\lambda D_j}}{2D_j}. \quad (23)$$

The general static solution in each medium j is then:

$$c_{j0}(z) = \hat{c}_j + B_{j0} e^{\beta_{j0}^+ z} + \tilde{B}_{j0} e^{\beta_{j0}^- z}, \quad (24)$$

where B_{j0} and \tilde{B}_{j0} are constants. Since $\beta_{j0}^- < 0$, a finite c_{j0} solution for $z = -\infty$ imposes $\tilde{B}_{20} = 0$. In addition, we have the boundary condition $c_{10}(z = 0) = c_e$ and the continuity of radon concentration and conservation of radon flux at $z = z_1$, which gives two additional conditions:

$$\begin{cases} c_{10}(z_1) = c_{20}(z_1) \\ \Phi_{10}(z_1) = \Phi_{20}(z_1) \end{cases} \quad (25)$$

Using eq. (6) and because of the continuity of F_j and c_j at the interface, the second equation of eq. (25) gives:

$$\varepsilon_1^g D_1^g \left. \frac{dc_{10}}{dz} \right|_{z=z_1} = \varepsilon_2^g D_2^g \left. \frac{dc_{20}}{dz} \right|_{z=z_1}. \quad (26)$$

The explicit solutions for the three constants B_{20} , B_{10} and \tilde{B}_{10} are given in Appendix A. Such multilayer calculations of the static radon concentration versus depth and of the static surface flux have been considered previously (Holford *et al.* 1993; Ho 2008; Antonopoulos-Domis *et al.* 2009; Girault & Perrier 2012a).

2.3.3 Fundamental and higher harmonics solution for radon concentration and flux

To obtain the general harmonic term $n \geq 1$, the harmonic terms of order n are identified in eq. (20), leading to:

$$\begin{aligned} c_{jn} i n \omega &= -\lambda c_{jn} - W_{j0} \left(\frac{dc_{jn}}{dz} + n \gamma_j (1+i) c_{jn} \right) + s_j (1+i) (A_j - B_j e^{-2\gamma_j (1+i) z}) \left(\frac{dc_{j(n-1)}}{dz} + (n-1) \gamma_j (1+i) c_{j(n-1)} \right) \\ &+ D_j \left(\frac{d^2 c_{jn}}{dz^2} + 2n \gamma_j (1+i) \frac{dc_{jn}}{dz} + 2i n^2 \gamma_j^2 c_{jn} \right), \end{aligned} \quad (27)$$

which can be rearranged into the following linear differential equation of the second order:

$$D_j \frac{d^2 c_{jn}}{dz^2} - X_{jn} \frac{dc_{jn}}{dz} - Y_{jn} c_{jn} = -s_j (1+i) (A_j - B_j e^{-2\gamma_j (1+i) z}) \left(\frac{dc_{j(n-1)}}{dz} + (n-1) \gamma_j (1+i) c_{j(n-1)} \right), \quad (28)$$

with

$$\begin{cases} X_{jn} = W_{j0} - 2D_j n \gamma_j (1 + i) \\ Y_{jn} = \lambda + ni\omega + W_{j0} n \gamma_j (1 + i) - 2D_j i n^2 \gamma_j^2. \end{cases} \tag{29}$$

The left-hand side of eq. (28) has general solutions of the form $c_{jn}(z) = e^{\beta_{jn}z}$ with:

$$D_j \beta_{jn}^2 - X_{jn} \beta_{jn} - Y_{jn} = 0, \tag{30}$$

which, using eq. (29), gives:

$$\beta_{jn}^{\pm} = \frac{W_{j0}}{2D_j} - n \gamma_j (1 + i) \pm \sqrt{\frac{W_{j0}^2}{4D_j^2} + \frac{\lambda + ni\omega}{D_j}}. \tag{31}$$

This expression is also valid for $n = 0$. Let us now prove that the general harmonic solution with $n \geq 1$ in each medium j can be expressed as a sum of M_n exponential terms:

$$c_{jn}(z) = \sum_{k=0}^{M_n-1} C_{jk}^n e^{\eta_{jk}^n z}, \tag{32}$$

where C_{jk}^n and η_{jk}^n are constants.

The form of eq. (32) and the expression of the constants can be found iteratively by imposing eq. (28). Indeed, let us assume that eq. (32) is valid at order $n - 1$ and that we know M_{n-1} and the constants C_{jk}^{n-1} and η_{jk}^{n-1} with $0 \leq k \leq M_{n-1} - 1$. The right-hand side of eq. (28) becomes:

$$-s_j(1 + i) (A_j - B_j e^{-2\gamma_j(1+i)z}) \sum_{k=0}^{M_{n-1}-1} C_{jk}^{n-1} (\eta_{jk}^{n-1} + (n - 1)\gamma_j(1 + i)) e^{\eta_{jk}^{n-1} z}, \tag{33}$$

hence a sum of $2M_{n-1}$ exponential terms.

A particular solution of eq. (28) can then be exhibited in the form:

$$\sum_{k=0}^{2M_{n-1}-1} C_{jk}^n e^{\eta_{jk}^n z}, \tag{34}$$

with, for $0 \leq k \leq M_{n-1} - 1$, the following parameters:

$$\eta_{jk}^n = \eta_{jk}^{n-1}, \tag{35}$$

$$C_{jk}^n = -s_j(1 + i) A_j \frac{\eta_{jk}^{n-1} + (n - 1)\gamma_j(1 + i)}{D_j \eta_{jk}^{n-2} - X_{jn} \eta_{jk}^n - Y_{jn}} C_{jk}^{n-1} \tag{36}$$

and, for $M_{n-1} \leq k \leq 2M_{n-1} - 1$:

$$\eta_{jk}^n = \eta_{jk}^{n-1} - 2\gamma_j(1 + i), \tag{37}$$

$$C_{jk}^n = s_j(1 + i) B_j \frac{\eta_{jk}^{n-1} + (n - 1)\gamma_j(1 + i)}{D_j \eta_{jk}^{n-2} - X_{jn} \eta_{jk}^n - Y_{jn}} C_{jk}^{n-1}. \tag{38}$$

The general solution of eq. (28), thus, is the sum of the general solution of the left-hand side of eq. (28) and the particular solution given by eq. (34):

$$c_{jn}(z) = \sum_{k=0}^{2M_{n-1}-1} C_{jk}^n e^{\eta_{jk}^n z} + B_{jn} e^{\beta_{jn}^+ z} + \tilde{B}_{jn} e^{\beta_{jn}^- z}, \tag{39}$$

where B_{j0} and \tilde{B}_{j0} are constants. This expression is of the form given by eq. (32) with:

$$M_n = 2M_{n-1} + 2, \tag{40}$$

$$\eta_{j(M_n-2)}^n = \beta_{jn}^+, \tag{41}$$

$$C_{j(M_n-2)}^n = B_{jn}, \tag{42}$$

$$\eta_{j(M_n-1)}^n = \beta_{jn}^-, \tag{43}$$

and

$$C_{j(M_n-1)}^n = \tilde{B}_{jn}. \tag{44}$$

Since $\beta_{jn}^- < 0$, a finite c_{jn} solution for $z = -\infty$ imposes $\tilde{B}_{2n} = 0$. The three constants B_{2n} , B_{1n} and \tilde{B}_{1n} are found, in terms of known quantities, by imposing the continuity of c_{jn} and the conservation of radon flux at $z = z_1$. The necessary manipulation of the continuity conditions and the explicit solutions for B_{2n} , B_{1n} and \tilde{B}_{1n} are given in Appendix A. Since $M_0 = 2$, according to eq. (40), for $n = 1$, the solution is a sum of 6 exponential terms, for $n = 2$, a sum of 14 terms, for $n = 3$, a sum of 30 terms and for $n = 4$, a sum of 62 terms.

3 RESULTS AND SENSITIVITY STUDIES IN THE CASE OF SLIGHT ADVECTION

In practice, some frequencies have a particular importance. The example, shown in Fig. 1, of a Fourier amplitude spectrum of the atmospheric pressure recorded in Paris (France), shows a dominating barometric tide S2 (12 hr), with a mean harmonic amplitude of 42 Pa (twice the amplitude in the power spectrum). Furthermore, the diurnal peak S1 is significant, with a mean amplitude 32 Pa. Peaks at 8 and 6 hr are also clear, with harmonic amplitudes of 13 and 6 Pa, respectively. A peak at 4 hr is barely visible, opening the possibility that a significant peak at 4 hr in a radon power spectrum could only be a harmonic 3 response from the soil to the S2 oscillation. The barometric tide S2 is more pronounced at lower latitudes (Simpson 1919; Lindzen & Chapman 1969). In the following, except when stated otherwise, we consider a S2 barometric oscillation with amplitude 100 Pa. This value is consistent with amplitude values considered by other workers (Holford *et al.* 1993).

We first examine some general aspects of the flow response to barometric oscillation in our soil + bedrock model, and then we turn to the radon response. Different situations are considered, with the numerical values of parameters given in Table 1. Case 1 corresponds to the commonly encountered situation of a permeable soil ($k_1 = 10^{-12} \text{ m}^2 = 1 \text{ D}$) over a moderately permeable bedrock ($k_2 = 2 \times 10^{-13} \text{ m}^2 = 200 \text{ mD}$), with typical effective radium content of 4 Bq kg^{-1} for the bedrock and 10 Bq kg^{-1} for the soil (Girault & Perrier 2011, 2012b; Girault *et al.* 2011). Case 2 describes the same soil, but over a bedrock as permeable as the soil. Case 3 corresponds to a homogeneous half-space having the parameters of the soil of case 1. Case 1B is an alternative of case 1 with the bedrock having low EC_{Ra} and case 2B is an alternative of case 2 with stronger static advection. Cases 4, 5 and 5B correspond to highly permeable soils and bedrocks, where very large permeability values are considered ($> 10^{-11} \text{ m}^2$, cases 4, 5 and 5B in Table 1), corresponding, for example, to a gravel layer over a sandy layer. Such situations are less likely to occur often in practice, but lead to spectacular effects.

3.1 Pore airflow

Pore airflow is sensitive to soil and bedrock permeability (Nilson *et al.* 1991; Holford *et al.* 1993). In the case of a moderately permeable bedrock ($k_2 = 2 \times 10^{-13} \text{ m}^2$ or 200 mD), the flow amplitude at the ground surface (Fig. 2a) is of the order of 0.04 cm d^{-1} at low soil permeability ($k_1 = 10^{-16} \text{ m}^2$ or 0.1 mD), increasing with soil permeability to a value of about 0.6 cm d^{-1} , independent of permeability, for

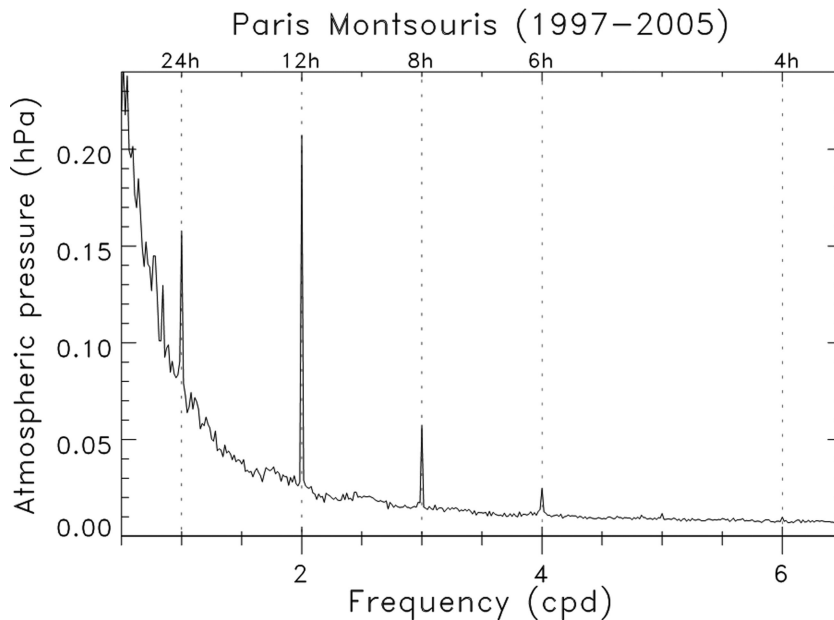


Figure 1. Fast Fourier Transform (FFT) amplitude spectrum of atmospheric pressure, recorded in Paris (France) from 1997 to 2005 with a sampling time of 1 hr (data from Météo-France), versus frequency expressed in cycles per day (cpd).

Table 1. Parameters and main results for the harmonic amplitudes $n \leq 4$ of radon flux and radon concentration at 30 and 65 cm depth, for various cases, and for a S2 surface barometric oscillation of 100 Pa amplitude. Bedrock/soil interface is located at 60 cm depth. Soil temperature is considered to be 10 °C, corresponding to a radon water to air partition coefficient of 0.35. Calculations correspond to the advective-diffusive model described in Section 2.

Quantities	Case 1 Permeable soil with moderately permeable bedrock	Case 1B with low radon source in bedrock	Case 2 Permeable soil with permeable bedrock	Case 2B with slight advection	Case 3 Identical permeable soil and bedrock	Case 4 Soil and bedrock with large permeability	Case 5 Soil with very large permeability	Case 5B with low radon source in bedrock
Soil properties:								
Permeability k_1 (m ²)	10 ⁻¹²		10 ⁻¹²		10 ⁻¹²	10 ⁻¹¹	10 ⁻¹⁰	
Porosity ε_1 (per cent)	25		25		25	40	35	
Saturation S_{w1} (per cent)	10		10		10	10	10	
EC_{Ra1} (Bq kg ⁻¹)	10		10		10	10	10	
Bedrock properties:								
Permeability k_2 (m ²)	2×10^{-13}		10 ⁻¹²		10 ⁻¹²	10 ⁻¹¹	10 ⁻¹¹	
Porosity ε_2 (per cent)	10		10		25	40	10	
Saturation S_{w2} (per cent)	50		50		10	50	50	
EC_{Ra2} (Bq kg ⁻¹)	4	0.2	4		10	0.2	4	0.2
Static flow (m s ⁻¹)	10 ⁻⁸		10 ⁻⁸	2×10^{-7}	10 ⁻⁸	10 ⁻⁸	10 ⁻⁸	10 ⁻⁸
Calculated soil parameters:								
Relative permeability	0.9		0.9		0.9	0.9	0.9	
Pneumatic diffusivity α_1 (m ² s ⁻¹)	0.022		0.022		0.022	0.14	1.6	
Radon diffusivity D_1 (m ² s ⁻¹)	2.5×10^{-6}		2.5×10^{-6}		2.5×10^{-6}	3.6×10^{-6}	3.3×10^{-6}	
Calculated bedrock parameters:								
Relative permeability	0.36		0.36		0.9	0.36	0.36	
Pneumatic diffusivity α_2 (m ² s ⁻¹)	8×10^{-3}		0.04		0.022	0.1	0.4	
Radon diffusivity D_2 (m ² s ⁻¹)	6.7×10^{-8}		6.8×10^{-8}		2.5×10^{-6}	9.4×10^{-7}	6.7×10^{-8}	
Static radon flux (10 ⁻³ Bq m ⁻² s ⁻¹)	26	22	26	47	43	18	24	20
Flux harmonic amplitudes:								
$n = 1$	0.26	0.29	0.50	0.39	3.6	1.4	0.22	0.93
$n = 2$	3.5×10^{-3}	1.6×10^{-3}	0.016	0.055	0.13	0.045	0.30	0.016
$n = 3$	9×10^{-5}	1.4×10^{-6}	9.6×10^{-4}	4.1×10^{-3}	2.2×10^{-3}	7.7×10^{-4}	0.06	6.6×10^{-4}
$n = 4$	1.8×10^{-6}	6.6×10^{-8}	4.2×10^{-5}	3×10^{-4}	10 ⁻⁵	8×10^{-6}	6.5×10^{-3}	6.6×10^{-5}
Concentration at 30 cm depth								
Static (Bq m ⁻³)	10 400	8600	10 400	20.4×10^3	19×10^3	2900	5200	4200
Harmonic amplitudes:								
$n = 1$	55	36	125	554	682	82	316	72
$n = 2$	2.7	0.02	13	42	7.3	0.59	115	1.8
$n = 3$	0.08	2.7×10^{-3}	0.88	2.7	0.27	0.05	26	0.25
$n = 4$	1.3×10^{-3}	4.8×10^{-5}	0.03	0.27	5.6×10^{-3}	10 ⁻³	2.4	0.024
Concentration at 65 cm depth								
Static (Bq m ⁻³)	51×10^3	10 100	51×10^3	127×10^3	34.8×10^3	3500	45×10^3	6000
Harmonic amplitudes:								
$n = 1$	4530	165	10 100	8700	470	53	34 000	350
$n = 2$	156	6.4	775	2100	4.9	6.2	8600	75
$n = 3$	22	0.86	242	124	0.11	0.18	8540	79
$n = 4$	1.7	0.065	41		3.2×10^{-3}	0.02	4600	42
Phase peak surface flow	0.343	0.344	0.360	0.360	0.375	0.371	0.367	0.367
Phase peak radon flux (harmonic $n = 1$)	0.420	0.435	0.440	0.482	0.485	0.452	0.600	0.453

soil permeability larger than 10^{-13} m² (100 mD). Amplitude is decreasing slowly with depth, with a stronger attenuation with depth at low soil permeability.

The effect of bedrock permeability on the specific flow is larger than the effect of soil permeability (Fig. 2b). For an almost impermeable bedrock ($k_2/k_1 < 10^{-4}$), specific flow at the ground surface is constant at 0.18 cm d⁻¹, basically imposed by the soil layer, with negligible motion in the bedrock. When the bedrock permeability becomes significant compared with the soil permeability ($k_2/k_1 > 0.1$), the amplitude of the flow increases proportionally to k_2 , and flow amplitude is hardly attenuated at typical soil depth values, which are also typical instrument positions. Thus, in a first approximation, it is the bedrock permeability that controls the amplitude of the flow, and, consequently the related advective transport of radon. Water content significantly affects airflow (Fig. S1) because of the same reason. Signatures of S2 advection in a

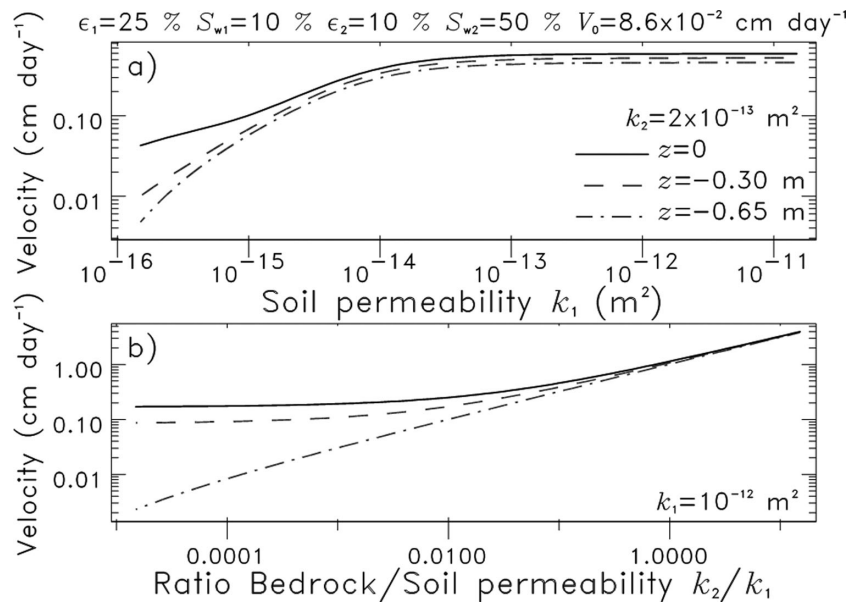


Figure 2. Harmonic 1 specific flow versus soil permeability (a) and versus the ratio of bedrock permeability to soil permeability (b), at the ground surface and at two depth positions (30 and 65 cm). Fixed parameters correspond to case 1 in Table 1. Soil thickness is 60 cm. Surface pressure oscillation is a S2 wave with 100 Pa amplitude.

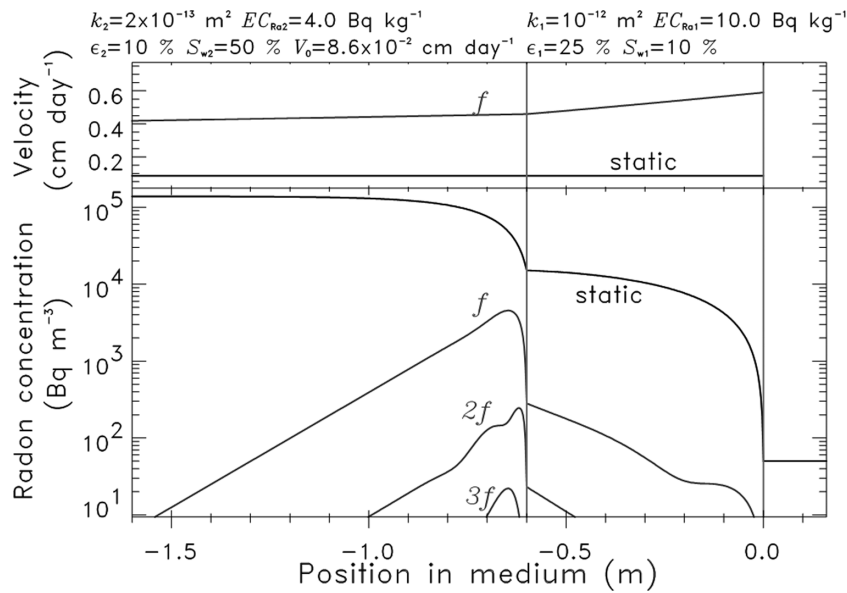


Figure 3. Static and harmonic amplitudes of specific flow (top plot) and radon concentration (bottom plot) versus position (depth) in the medium. Fundamental term is indicated by f and harmonic n by nf . The parameters of the bedrock and soil layer, indicated at the top, correspond to case 1 in Table 1. Static advective Darcy velocity is $V_0 = 10^{-8} \text{ m s}^{-1}$.

soil indicate sufficiently large soil permeability and the presence of sufficiently thick permeable bedrock. This statement needs to be revised in the presence of near-surface water table (Nilson *et al.* 1991; Holford *et al.* 1993; Robinson *et al.* 1997). Nevertheless, in the following and when analysing radon harmonics, we can rely on this guiding principle.

3.2 Harmonic amplitude of radon concentration versus position

The effect of barometric pumping on radon concentration varies strongly with depth (Figs 3–7). In case 1 (Fig. 3), the attenuation of the pressure wave is moderate in the bedrock and the amplitude of the first harmonic of the flow, of the order of $0.4\text{--}0.6 \text{ cm d}^{-1}$, dominates over the static Darcy velocity, negligible in this configuration. Radon concentration is large at depth in the bulk of the bedrock, of the order of $150 \times 10^3 \text{ Bq m}^{-3}$, with a rapid decrease to $15 \times 10^3 \text{ Bq m}^{-3}$ at the interface with the soil. The amplitude of the first harmonic of the concentration shows a notable spatial variation: increasing slowly when penetrating into the soil layer to a maximum value of 282 Bq m^{-3} , at the interface, and showing a rapid increase in the bedrock to a large maximum value of about 4500 Bq m^{-3} , 5 cm below the interface,

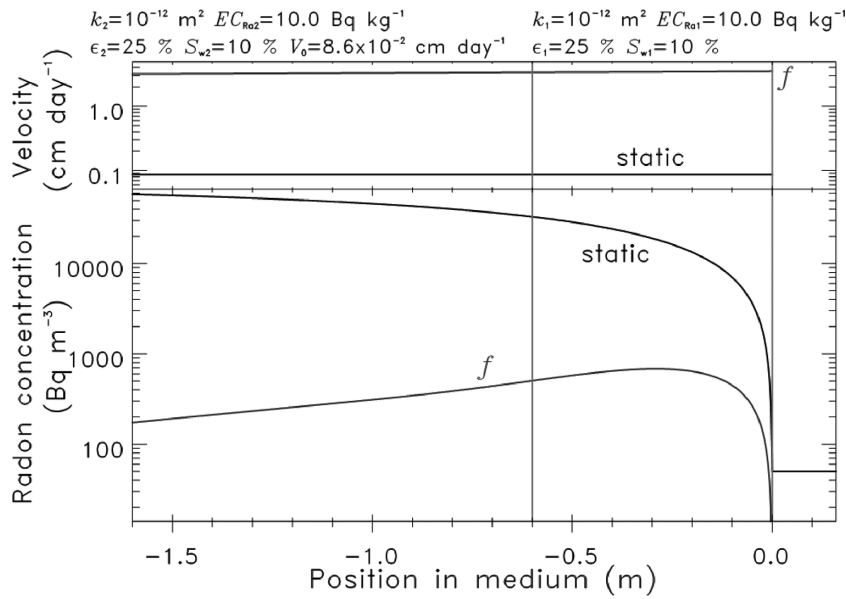


Figure 4. Static and harmonic amplitudes of specific flow (top plot) and radon concentration (bottom plot) versus position (depth) in the medium. Fundamental term is indicated by f and harmonic n by nf . The parameters of the bedrock and soil layer, indicated at the top, are identical and correspond to case 3 (homogeneous half-space) in Table 1. Static advective Darcy velocity is $V_0 = 10^{-8} \text{ m s}^{-1}$.

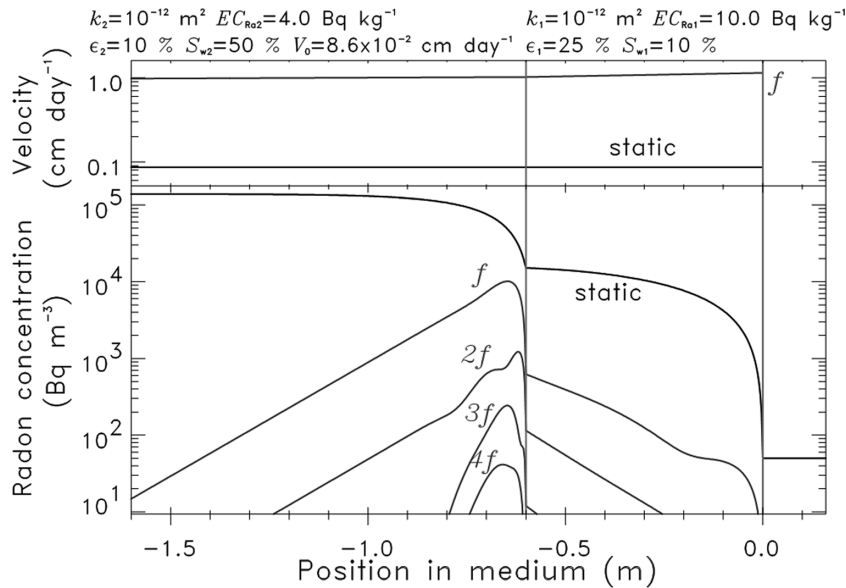


Figure 5. Static and harmonic amplitudes of specific flow (top plot) and radon concentration (bottom plot) versus position (depth) in the medium. Fundamental term is indicated by f and harmonic n by nf . The parameters of the bedrock and soil layer, indicated at the top, correspond to case 2 (permeable bedrock) in Table 1. Static advective Darcy velocity is $V_0 = 10^{-8} \text{ m s}^{-1}$.

followed by an exponential attenuation below this maximum. The second harmonic, with a maximum of 246 Bq m^{-3} in the bedrock, 2 cm below the soil interface, should also be visible in an amplitude spectrum, while the third harmonic, with a maximum of 22 Bq m^{-3} , 5 cm below the soil in the bedrock, is not insignificant. Our calculation, thus, shows that, in a bedrock + soil configuration, fundamental and higher harmonic amplitudes of radon concentration are largest just below the interface, with rapid reductions around the maximum. Exact depth of the instruments then becomes a critical issue to be aware of.

The situation is radically different in a homogeneous half-space (case 3, Fig. 4). Only the amplitude of the fundamental is significant and it is largest in the vicinity of the surface, with a maximum of 682 Bq m^{-3} at 30 cm depth, but rather constant between 50 and 15 cm depth. The enhancement of the harmonic response in case 1, compared with the homogeneous half-space, is therefore essentially due to the strong gradient of the static radon concentration in the vicinity of the interface. Thus, large amplitude of the radon concentration results not only from the presence of penetrating flow, due to a permeable basement, but, also, and mainly, from the presence of conditions creating large gradients of static radon concentration.

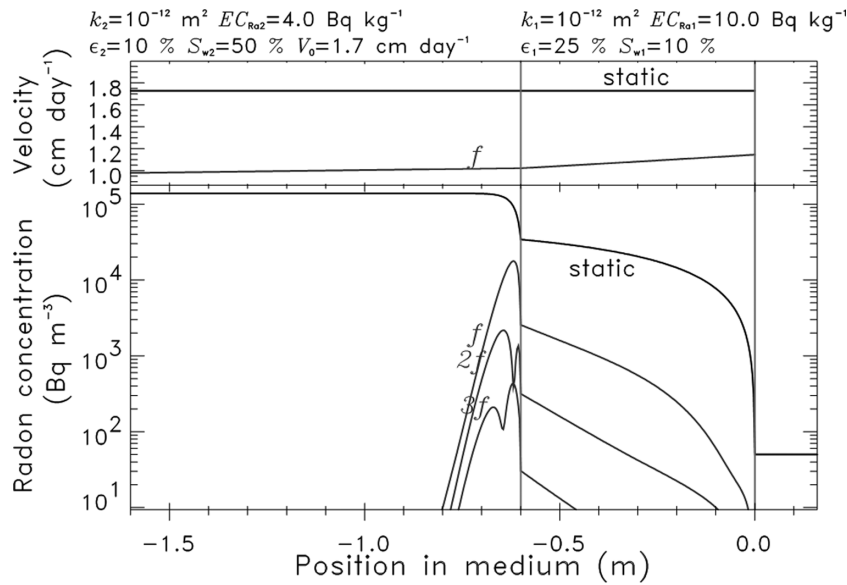


Figure 6. Static and harmonic amplitudes of specific flow (top plot) and radon concentration (bottom plot) versus position (depth) in the medium. Fundamental term is indicated by f and harmonic n by nf . The parameters of the bedrock and soil layer, indicated at the top, correspond to case 2B (permeable bedrock with slight advection) in Table 1. Static advective Darcy velocity is $V_0 = 2 \times 10^{-7} \text{ m s}^{-1}$.

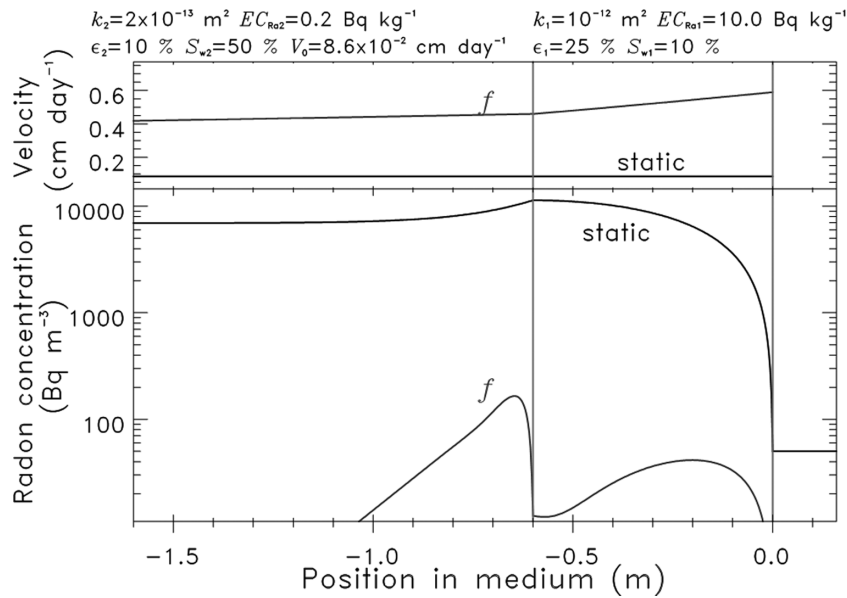


Figure 7. Static and harmonic amplitudes of specific flow (top plot) and radon concentration (bottom plot) versus position (depth) in the medium. Fundamental term is indicated by f . The parameters of the bedrock and soil layer, indicated at the top, correspond to case 4 (very permeable bedrock and soil, negligible radon production in bedrock) in Table 1. Static advective Darcy velocity is $V_0 = 10^{-8} \text{ m s}^{-1}$.

Larger bedrock permeability, in the presence of similar static gradients as case 1, results in larger harmonic amplitude (case 2, Fig. 5). In this case, the maximum fundamental response is $10 \times 10^3 \text{ Bq m}^{-3}$ and occurs, again, in the bedrock, 5 cm below the soil interface, while the predicted amplitudes of higher harmonics $n = 2, 3$ and 4 are larger than 40 Bq m^{-3} (Table 1).

In the presence of slight advection ($V_0 = 10^{-7} \text{ m s}^{-1}$, case 2B in Table 1), radon concentration distributions are squeezed from below against the bedrock/soil interface (Fig. 6). The maximum fundamental response now becomes $18 \times 10^3 \text{ Bq m}^{-3}$, 3 cm below the interface, and the first harmonic to about 2170 Bq m^{-3} , occurring 5 cm below the interface. The response in the soil is also significantly enhanced, with fundamental amplitude larger than 200 Bq m^{-3} from 60 to 18 cm depth.

When radon production in the bedrock is small (case 4, Fig. 7), the static radon concentration near-surface and radon flux at the surface remain similar ($22 \times 10^{-3} \text{ Bq m}^{-2} \text{ s}^{-1}$ compared with $26 \times 10^{-3} \text{ Bq m}^{-2} \text{ s}^{-1}$ for the flux, see Table 1), but the spatial variation of the harmonic response is completely different, with all harmonics becoming negligible except the fundamental. Now, the fundamental shows two maxima: one in the bedrock, with peak amplitude 165 Bq m^{-3} , 5 cm below the interface, and one in the soil, with peak amplitude 41 Bq m^{-3} , 20 cm below surface. While the static distribution in the soil is similar in cases 1 and 4, the response to the S2 oscillation is

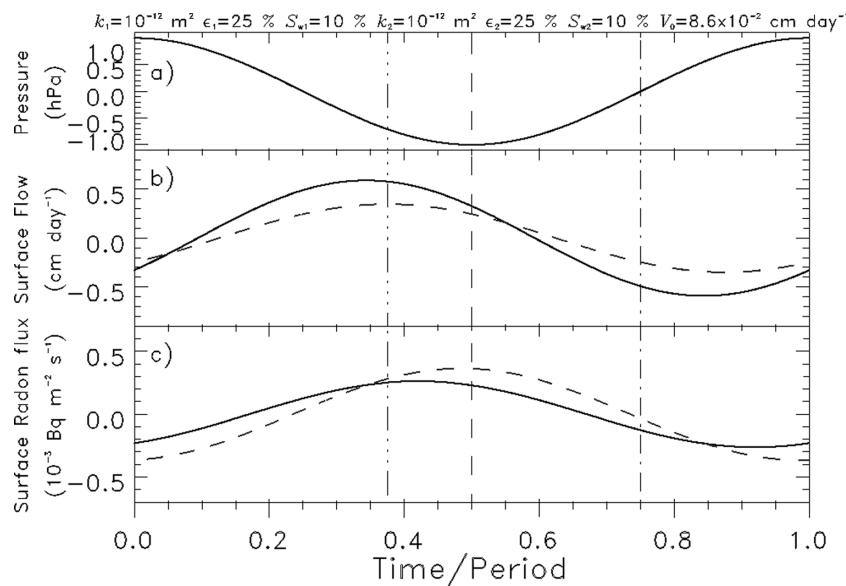


Figure 8. Temporal variation in one period of atmospheric pressure (a), surface specific flow (b) and surface radon flux (c). Full line corresponds to case 1 in Table 1 and the dashed line to uniform half-space (case 3 in Table 1). To allow comparison with case 1, amplitudes of specific flow and radon flux for the uniform half-space have been divided by 10.

completely different. Thus, measuring the S2 response, even in the shallow soil region, potentially provides a probe of both shallow and deeper radon sources.

When larger permeability values are considered ($>10^{-11} \text{ m}^2$, cases 4, 5 and 5B in Table 1), the harmonic response for the S2 oscillation can reach significant values for concentrations for all orders $n \leq 4$ (Table 1), but only when a significant radon source is present in the bedrock. By contrast, response for the surface radon flux remains small, except for the fundamental in case 4, which is then about 10 per cent of the static amplitude, similar to the case of a homogeneous half-space (case 3).

Another possibility to obtain large barometric response is the presence of anomalously large effective radium concentrations. Values of EC_{Ra} larger than 100 Bq kg^{-1} for the soil are rare, but nevertheless can occur in natural conditions (Nguyen *et al.* 2005; Sakoda *et al.* 2010; Girault & Perrier 2012b), and also, for example, in the case of former industrial sites with layers of uranium mill tailings (White & Rood 2001; Ferry *et al.* 2002; Gutiérrez *et al.* 2004). When, in the conditions of case 1, we take 100 Bq kg^{-1} for the soil layer, the static flux becomes $228 \times 10^{-3} \text{ Bq m}^{-2} \text{ s}^{-1}$, and the amplitude of the first harmonic 357 Bq m^{-3} at 30 cm depth and 838 Bq m^{-3} at 65 cm depth. More spectacular enhancements are observed when the value of 100 Bq kg^{-1} is taken for the bedrock. Then, the amplitude of the first harmonic becomes 1340 Bq m^{-3} at 30 cm depth and $120 \times 10^3 \text{ Bq m}^{-3}$ at 65 cm depth, for a static flux of $114 \times 10^{-3} \text{ Bq m}^{-2} \text{ s}^{-1}$. This illustrates again the sensitivity of the barometric response to conditions at depth, while the static flux is more sensitive to the conditions in the soil. Such high values of EC_{Ra} are not necessarily rare for rocks, even in the absence of uranium ore (Stranden *et al.* 1984; Sakoda *et al.* 2008; Lee *et al.* 2010; Girault & Perrier 2012b).

3.3 Phase of the first harmonic of radon flux and concentration

Significant information is also contained in the phase (Fig. 8). In a homogeneous half-space (case 3, dashed lines), the surface-specific flow response lags behind pressure by $3/8$ of a period, as it is well known for heat flux (Carslaw & Jaeger 1946). Radon flux at the surface, by contrast, lags behind pressure by about half a period.

The relative phases are different in the case of a bedrock/soil interface (case 1, full lines in Fig. 8). Specific flow lags behind pressure by about 0.343 period, instead of $3/8$, and surface radon flux by 0.42 period. While the phase shift in the presence of shallow heterogeneity is not tremendous, it might be sufficient to be observable. Recent experimental observations with CO_2 flux in the Azores archipelago (Rinaldi *et al.* 2012), while complicated by other effects, suggest lag times of the order of 6 hr, similar to the predictions of our model. Such promising observations suggest that precise experimental data soon will be available to test the various analytical or numerical models. Techniques allowing the observation of phases in small oscillatory signals (Groves-Kirkby *et al.* 2006) then will be of great help.

3.4 Response attenuation versus harmonic order

The relative amplitudes of the fundamental and of the higher harmonics are meaningful. Let us first consider the first harmonics ($n \leq 4$) for various pressure oscillations in case 1 (Fig. 9). We consider the main peaks observed in a typical atmospheric pressure time-series (Fig. 1), and we compare the various amplitudes of response versus frequency. For surface radon flux, the main response is the fundamental of the S2 oscillation, with amplitude of about $0.26 \times 10^{-3} \text{ Bq m}^{-2} \text{ s}^{-1}$, which, however, may not be easy to detect experimentally given the difficulties

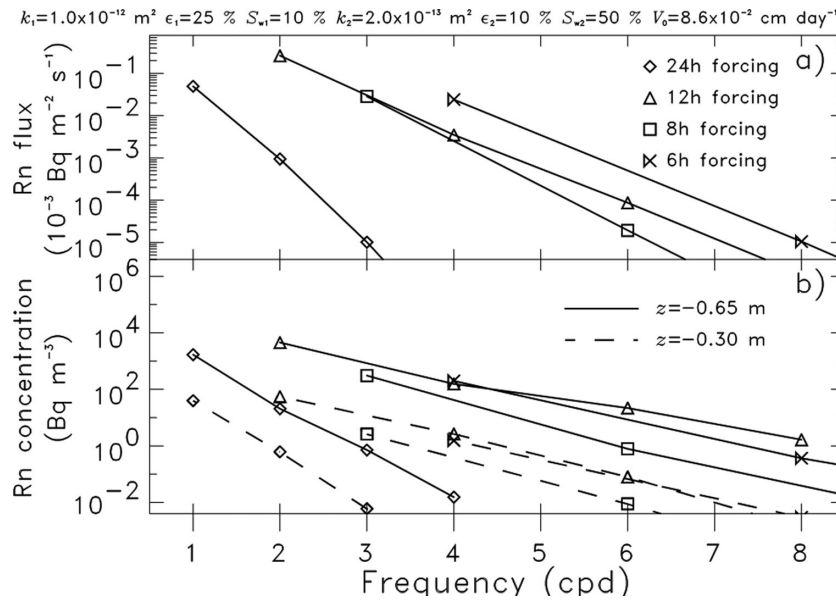


Figure 9. Harmonic amplitudes versus frequency for radon surface flux (a) and radon concentration at two depth values (b) for a 24 hr barometric oscillation with 30 Pa amplitude (diamonds), a 12 hr barometric oscillation with 100 Pa amplitude (triangles), a 8 hr barometric oscillation with 16 Pa amplitude (squares) and a 6 hr barometric oscillation with 6 Pa amplitude (knots). The parameters of the bedrock and soil layer, indicated at the top, correspond to case 1 (moderately permeable bedrock below permeable soil, common radon production in bedrock) in Table 1.

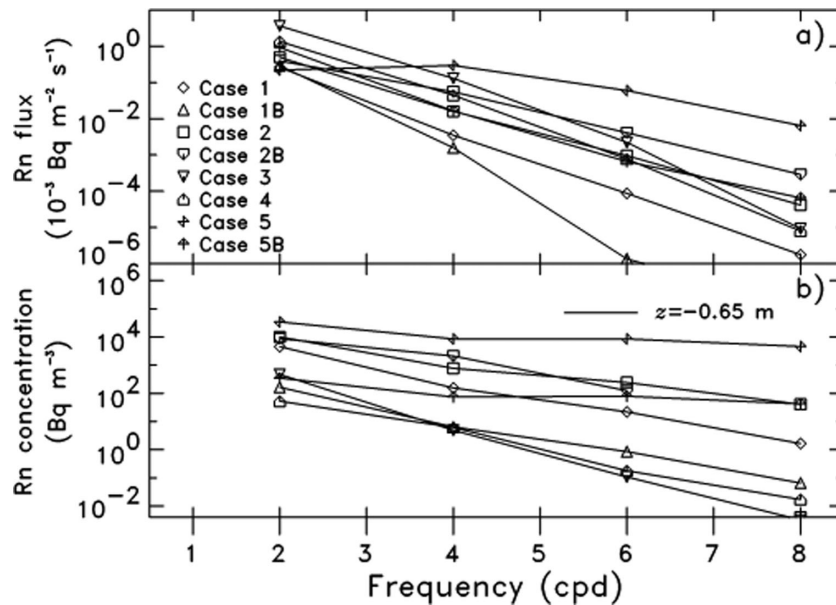


Figure 10. Harmonic amplitudes versus frequency for radon surface flux (a) and radon concentration at a depth of 65 cm (b) for a 12 hr barometric oscillation with 100 Pa amplitude for the various cases considered in Table 1.

in measuring radon flux (Girault *et al.* 2009). The second harmonic of the S3 response is of the same order of magnitude as the third harmonic of the S2 response, both being, however, extremely small.

Larger and more surprising effects are noted when looking at the harmonic responses of concentration (Fig. 9b). At the critical depth of 65 cm, not only the fundamental responses at 24, 12, 8 and 6 hr should be easily detectable, with amplitudes larger than 50 Bq m^{-3} , but some higher harmonics as well. The decrease of amplitude with increasing order is less pronounced for S2 than for S1. Higher frequencies, thus, tend to enhance non-linear couplings and the generation of higher harmonics. Remarkably, the third harmonic of the S2 oscillation, with amplitude of 162 Bq m^{-3} at 65 cm depth, should be detectable and, furthermore, dominates the second harmonic of the S3 oscillation. Thus, the 4 hr peak, in this case, is predicted to be almost purely the third harmonic of the S2 wave.

The fundamental and the higher harmonics are sensitive to the bedrock parameters and the presence of advection, even slight (Fig. 10). The amplitudes vary by almost two orders of magnitude, both for the surface flux and the concentration at the critical depth of 65 cm (Fig. 10b). Cases providing large amplitudes in the surface flux (cases 3 and 4, corresponding to permeable and very permeable bedrock) are not cases yielding the largest amplitudes in the concentration, which are cases 2, 2B and 1. Thus, while obtaining time-series of radon flux

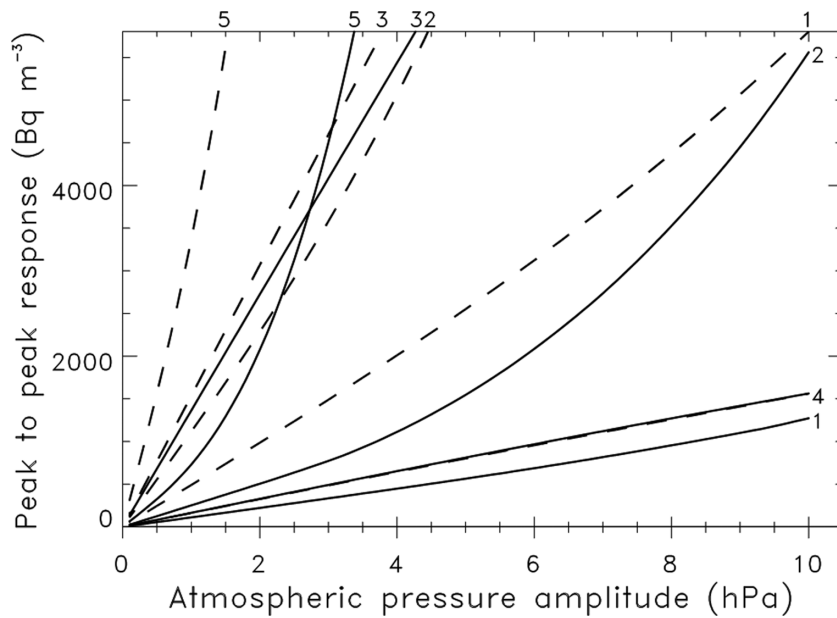


Figure 11. Peak to peak amplitude of the radon concentration response at 30 cm depth, including harmonics n up to degree 5, for the various cases considered in Table 1 with negligible advection ($V_0 = 10^{-8} \text{ m s}^{-1}$, full line), and with slight advection ($V_0 = 10^{-7} \text{ m s}^{-1}$, dashed line). The label numbers at the top and the side refer to the cases.

is difficult, comparing the peaks in flux and concentration spectra would provide critical constraints on the parameters of the shallow versus deeper subsurface.

Case 5 provides an example where the largest response in the flux is in the second harmonic (see Table 1), with significant third- and fourth-order response in the concentration. This case illustrates in a spectacular manner the non-linear nature of the advection-diffusion problem and that, in some cases, a first-order calculation can be incorrect. The non-linearity of the response is further displayed in Fig. 11, which shows the amplitude of the concentration response versus the amplitude of the barometric oscillation, with or without advection. While some conditions lead to an almost linear response (cases 1, 3 and 4), a pronounced non-linear response appears for cases 2 and 5. The presence of slight advection in case 2 restores a linear trend. Non-linearity, thus, is not necessarily associated with a large response.

3.5 Sensitivity of radon flux and concentration harmonic responses to model parameters

The static and harmonic responses to the S2 oscillation for the surface radon flux and radon concentration at a typical depth are modified by advection in different manners. In Fig. 12, the effect of the static advection is studied for case 4, for which the accessible range of V_0 values is larger. Indeed, instabilities tend to appear in the calculations when V_0 is larger than 10^{-6} m s^{-1} . While the static radon flux at the surface is increasing with increasing advection (Fig. 12a), the harmonic amplitudes are not changed by more than a factor of 2–4. Thus, the harmonic amplitudes are more sensitive to the presence of bedrock radon sources (case 1 versus case 1B) than to the presence of advection. For large values of V_0 , the amplitudes converge to the amplitudes obtained in a purely advective calculation (see below).

Not only the bedrock radon source term bears a crucial importance on the harmonic amplitudes, but also the properties of bedrock and soil, for example, water saturation of bedrock (Fig. 13). Water saturation affects both the pneumatic diffusivity (eq. 2) and the radon diffusion coefficient (see Section 2.1). The effect of water saturation on the source term (eq. 4) plays only a secondary role. Thus, two main effects compete in Fig. 13. At low bedrock water saturation, the harmonic amplitudes are enhanced by about a factor of 10, compared with the minimum, because radon diffusion coefficient is larger. At large bedrock water saturation, the amplitudes increase because the flow gets more confined near the soil interface, where static concentration gradients are important.

The effect of other parameters depends on the conditions (Figs S2–S6). In all cases, while subsurface parameters can have important effects on the static and harmonic responses, static and harmonic parameters of flux and concentration tend to react in different ways. When advection is not significant, bedrock porosity, for example, has a notable effect on the harmonic 1 response only (Fig. 14). Larger bedrock porosity indeed produces larger flux response, a situation opposite to the situation for radon concentration at depth discussed previously. The effect is significant only when the bedrock is sufficiently permeable (case 2, permeable bedrock), but not otherwise (case 1). However, the effect of bedrock porosity is only negligible for the radon flux in the absence of advection. Indeed, the presence of a slight advection tends to stretch the distributions. Thus, the experimental measurement of these quantities could lead to decipherable information on the structure of the deeper subsurface using very shallow measurements.

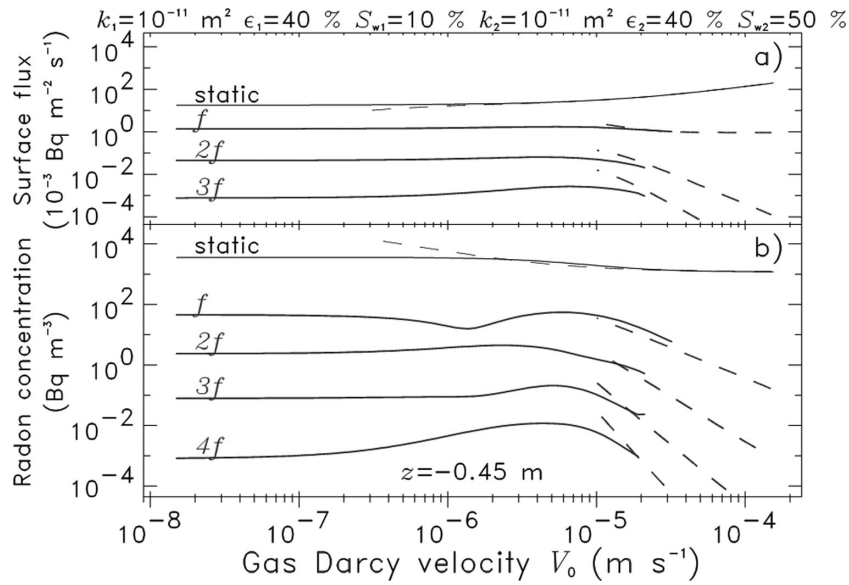


Figure 12. Static and harmonic amplitudes of surface radon flux (a) and radon concentration at 45 cm depth (b) versus static specific flow. The full lines correspond to the advective-diffusive model (Section 3) and the dashed lines to the purely advective model (Section 4). Conditions refer to case 4 in Table 1 and a S2 oscillation with 100 Pa amplitude.

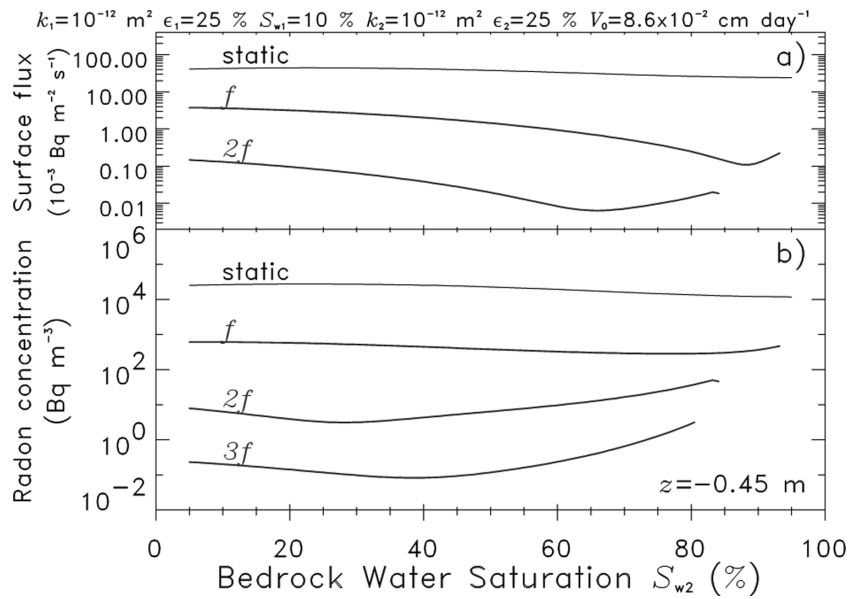


Figure 13. Static and harmonic amplitudes of surface radon flux (a) and radon concentration at 45 cm depth (b) versus bedrock water saturation. Conditions refer to case 2 in Table 1 and a S2 oscillation with 100 Pa amplitude.

4 HARMONIC RESPONSE IN THE PRESENCE OF STRONG ADVECTION

The case of large V_0 values is relevant for degassing hydrothermal systems and active volcanoes, and deserves a dedicated treatment. The above calculations, indeed, are not adequate because of numerical instabilities appearing for values of V_0 larger than 10^{-6} or 10^{-4} m s^{-1} , depending on the considered case. More appropriate analytical expressions can be derived when diffusion effects can be neglected.

Let us consider N porous media separated by $N - 1$ horizontal interfaces z_j , with $0 \leq j \leq N - 2$. Medium j corresponds to $z_j < z < z_{j-1}$ for $1 \leq j \leq N - 2$. Medium 0 corresponds to $z_0 < z < 0$ and medium $N - 1$ to $z < z_{N-2}$. While, in principle, we can solve the flow problem for N layers without difficulties (Perrier & Richon 2010, Appendix A), in this paper, we consider the case where permeability and air-filled porosity for layer $j \geq 2$ are the same as layer $j = 1$, so that we can continue to use the solution given in Section 2. In the applications considered below, we mainly consider additional layers for the radon source term, without further complications for the propagation of the pressure wave. In the following, quantities referring to the purely advective limit case are distinguished from the previous advective-diffusive case by adding a bar above the symbols. The details of the calculation are given in Appendix B. We assume here that spatial and temporal pressure variations remain sufficiently small, so that the linear eq. (1) remains valid.

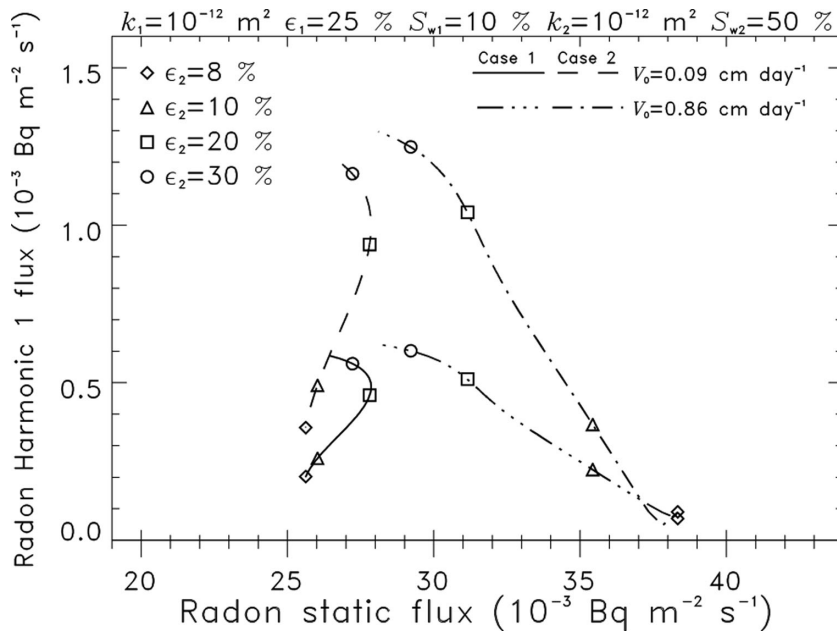


Figure 14. Fundamental (harmonic $n = 1$) response of surface radon flux versus static radon flux with changing bedrock porosity. Cases 1 and 2 from Table 1 are considered with negligible ($10^{-8} \text{ m s}^{-1} \cong 0.09 \text{ cm d}^{-1}$) or slight ($10^{-7} \text{ m s}^{-1} \cong 0.86 \text{ cm d}^{-1}$) static advection.

The purely advective case, with $N = 2$, and the high V_0 limit of the advective-diffusive case described in Section 2, overlap when they have a common domain of validity, around $V_0 = 10^{-5} \text{ m s}^{-1}$ (Fig. 12). In the limit of high advection, the harmonic amplitudes of radon concentration fall with increasing V_0 , and reach negligible values when V_0 is of the order of 10^{-4} m s^{-1} , corresponding to static radon flux larger than about $500 \times 10^{-3} \text{ Bq m}^{-2} \text{ s}^{-1}$. The harmonics of the surface flux also decrease rapidly, except the fundamental, which appears to be constant versus V_0 in Fig. 12(a). Indeed, at large V_0 , the fundamental response of radon flux has a constant limit given by:

$$\Phi_{s1}|_{V_0 \rightarrow \infty} = -s_1 \varepsilon_1^g (1 + i) (A_1 - B_1) \hat{c}_2. \quad (45)$$

This result, nevertheless, has to be taken with proper caution, because eq. (1) assumes a linear behaviour of the pressure field, a hypothesis that might need to be questioned in particular cases with large advection velocities.

In the following, we consider the situation $N = 3$. This allows us to evaluate the effect of a deep basement, in which the oscillation of the flow is assumed to be zero, on the surface radon flux and shallow radon concentration. We consider that the basement is at 500 m and we compare two situations (Table 2). In case A1, we have $EC_{\text{Ra}3} = 0.2 \text{ Bq kg}^{-1}$, and the radon sources, consequently, are confined to the shallow bedrock and the soil. In case A2, by contrast, we have $EC_{\text{Ra}3} = 10 \text{ Bq kg}^{-1}$, illustrating a situation with significant radon sources at depth. Results for the static and harmonic $n = 1$ components are given in Table 2.

The fundamental component of the specific flow and the static and fundamental harmonic of radon concentration are shown versus position in the medium in Fig. 15 for case A1 (shallow radon sources). In this case, static radon concentration is imposed by the term \hat{c}_2 in the case of moderate advection ($V_0 = 10^{-5} \text{ m s}^{-1}$), giving a concentration of $70 \times 10^3 \text{ Bq m}^{-3}$ in the shallow bedrock and the soil (Fig. 15b). This value is reduced by about a factor of 2 when advection is larger ($V_0 = 10^{-4} \text{ m s}^{-1}$), producing a static surface radon flux of $3.9 \text{ Bq m}^{-2} \text{ s}^{-1}$, instead of $0.7 \text{ Bq m}^{-2} \text{ s}^{-1}$ for $V_0 = 10^{-5} \text{ m s}^{-1}$. While the bedrock/soil interface does not play any role in the static radon concentration, indicating that radon production in the soil is negligible in the high-advection limit, the fundamental harmonic of radon concentration is enhanced in the vicinity of the interface, especially for moderate advection, and reaches values of the order of 5 Bq m^{-3} , maybe detectable in favourable circumstances. In the case of high advection (Fig. 15b, dashed line), the amplitude is strongly reduced to values smaller than 0.5 Bq m^{-3} , below likely detection. The fundamental amplitude of the flux (Table 2) amounts to $9.2 \times 10^{-3} \text{ Bq m}^{-2} \text{ s}^{-1}$ for $V_0 = 10^{-5} \text{ m s}^{-1}$. This value is significant, but it is about 1.3 per cent of the static flux, and, hence, probably impossible to detect. This amplitude is even smaller when larger static flow values are considered (Table 2).

The picture is qualitatively different in the case of deep radon sources (case A2, Fig. 16). In this case, static radon concentration is increased when larger static advective flows are considered (Fig. 16c). The fundamental amplitude of radon concentration (Fig. 16b), by contrast, is decreasing when static advective flow is increased (dashed line), but the effect is less pronounced than in the case A1 (Fig. 15b) and the amplitude remains larger than 2 Bq m^{-3} . Thus, a fundamental S2 response in radon concentration in the shallow soil, in presence of large static advection, would be an indication for the presence of deep radon sources, because this situation cannot occur in the presence of shallow radon sources only (case A1). This calculation, thus, suggests that searching for small S2 response in radon concentration time-series is meaningful, even in the case of large advection. As for the fundamental harmonic in the surface radon flux (Table 2), while its value is significant (larger than about $10 \times 10^{-3} \text{ Bq m}^{-2} \text{ s}^{-1}$) and increasing with V_0 , it is a negligible fraction (below 1 per cent or even smaller than 10^{-3}) of the static flux.

Table 2. Parameters and main results for the harmonic amplitudes $n \leq 4$ of radon flux and radon concentration at 30 and 65 cm depth, for various cases, and for a S2 surface barometric oscillation of 100 Pa amplitude. Deep bedrock is located below a depth of 500 m. Bedrock/soil interface is located at 60 cm depth. Soil temperature is considered to be 10 °C, corresponding to a radon water to air partition coefficient of 0.35. Calculations correspond to the purely advective model described in Section 4.

Quantities	Case A1			Case A2		
	Shallow radon source			Deep radon source		
Soil properties:						
Permeability k_1 (m ²)	10 ⁻¹²			10 ⁻¹²		
Porosity ε_1 (per cent)	25			25		
Saturation S_{w1} (per cent)	10			10		
EC_{Ra1} (Bq kg ⁻¹)	10			10		
Shallow bedrock properties:						
Permeability k_2 (m ²)	10 ⁻¹²			10 ⁻¹²		
Porosity ε_2 (per cent)	10			10		
Saturation S_{w2} (per cent)	50			50		
EC_{Ra2} (Bq kg ⁻¹)	2			2		
Deep bedrock properties:						
Porosity ε_3 (per cent)	10			10		
Saturation S_{w3} (per cent)	50			50		
EC_{Ra3} (Bq kg ⁻¹)	0.2			10		
Static flow (m s ⁻¹)	10 ⁻⁵	10 ⁻⁴	10 ⁻³	10 ⁻⁵	10 ⁻⁴	10 ⁻³
Static radon flux (10 ⁻³ Bq m ⁻² s ⁻¹)	697	3900	11 400	700	21 000	340 000
Flux harmonic amplitude $n = 1$ (10 ⁻³ Bq m ⁻² s ⁻¹)	9.2	5.2	1.5	9.3	28	45

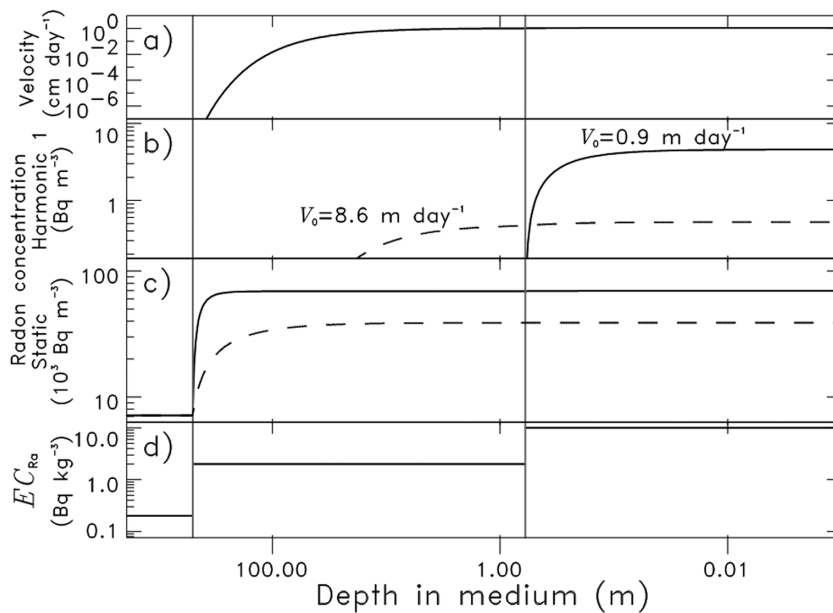


Figure 15. Harmonic 1 of specific flow rate (a), radon concentration (b), static radon concentration (c) and spatial structure of EC_{Ra} (d) versus position in the medium, for the case of shallow radon sources (case A1 in Table 2). Deep rock basement is located at 500 m depth below surface and bedrock/soil interface at 60 cm depth. Full lines of radon concentration correspond to a static advection of 10⁻⁵ m s⁻¹ (0.9 m d⁻¹) and dashed lines to 10⁻⁴ m s⁻¹ (8.6 m d⁻¹).

The two cases A1 and A2 are compared in Fig. 17, which shows the fundamental harmonic of the radon flux versus static radon flux, with changing bedrock porosity. Reduction of bedrock porosity leads to strong enhancement of both static and fundamental harmonic of radon flux, a situation qualitatively different from the situation dominated by diffusion, with low advection (Fig. 14). In the case of shallow radon sources (case A1), the harmonic 1 amplitudes remain smaller than 20×10^{-3} Bq m⁻² s⁻¹, even in the presence of large advection. In the case of deep radon sources (case A2), harmonic 1 amplitudes larger than 70×10^{-3} Bq m⁻² s⁻¹ are possible when the bedrock porosity is small. In all cases, static radon flux and its harmonic 1 both remain small when the bedrock porosity is larger than 25 per cent, a situation which is not very common in practice, but nevertheless possible.

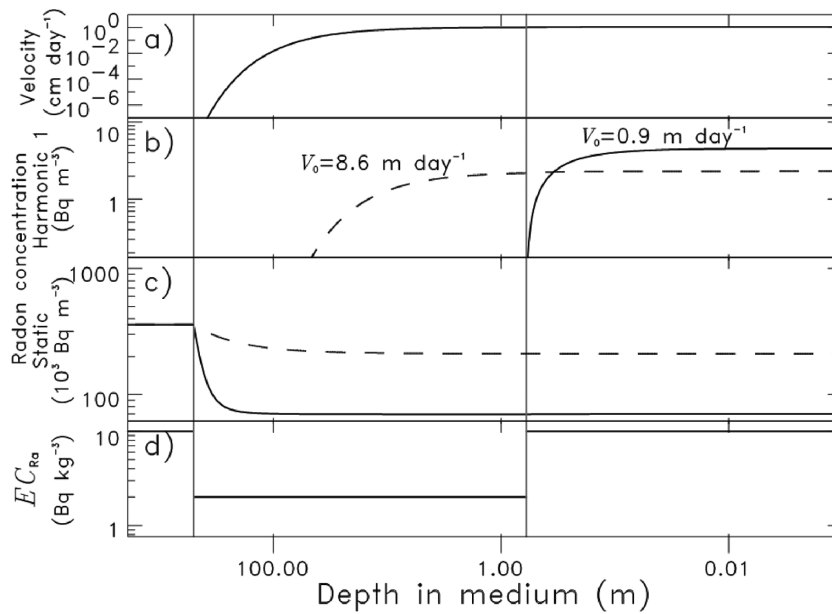


Figure 16. Harmonic 1 of specific flow rate (a), radon concentration (b), static radon concentration (c) and spatial structure of EC_{Ra} (d) versus position in the medium, for a case with deep radon sources (case A2 in Table 2). Deep rock basement is located at 500 m depth below surface and bedrock/soil interface at 60 cm depth. Full lines of radon concentration correspond to a static advection of 10^{-5} m s^{-1} (0.9 m d^{-1}) and dashed lines to 10^{-4} m s^{-1} (8.6 m d^{-1}).

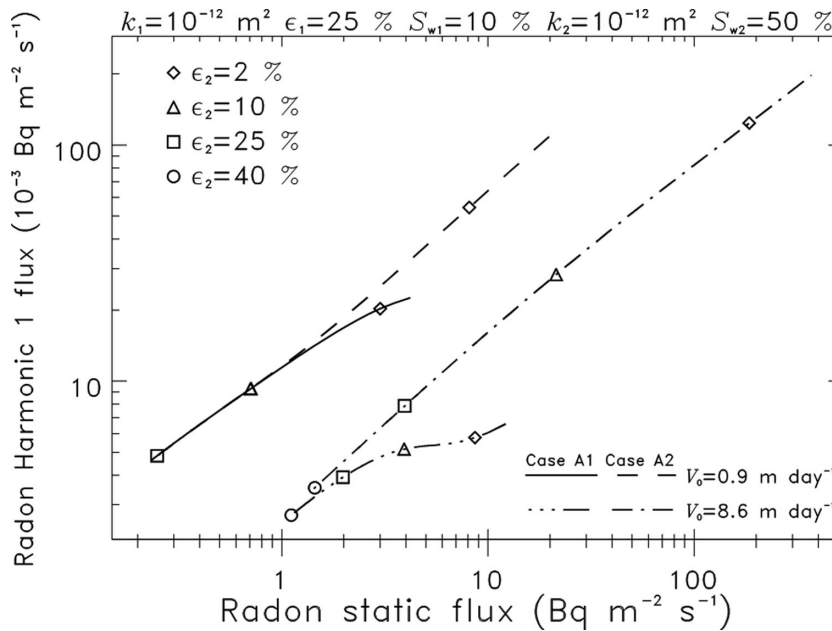


Figure 17. Fundamental (harmonic $n = 1$) response of surface radon flux versus static radon flux with changing bedrock porosity. Cases A1 and A2 from Table 2 are considered with significant ($10^{-5} \text{ m s}^{-1} \cong 0.9 \text{ m d}^{-1}$) or large ($10^{-4} \text{ m s}^{-1} \cong 8.6 \text{ m d}^{-1}$) static advection.

5 DISCUSSION AND EXAMPLES OF APPLICATIONS

The analytic calculations presented in this paper are useful to understand the meaning of the presence or absence of peaks in the amplitude spectrum of experimental radon time-series, as well as their temporal variations. The situation considered here of a homogeneous soil layer over homogeneous bedrock, while an oversimplification of the natural context, is probably sufficient at the current stage. The results obtained in selected situations (Tables 1 and 2) provide important guidelines to install the instruments in relevant locations. One of the main results is that the harmonic responses, while not necessarily large in the soil layer, are strongly enhanced in the bedrock, just below the soil interface. This barometric sensitive zone, with a thickness of a few centimetres, is specific to radon-222 and is also extremely sensitive to the transport properties of the media, beyond simply the radon source term EC_{Ra} . While more difficult to observe, harmonic response is also present in the radon surface flux, with signatures, which are usually complementary to the signatures observed in radon concentration.

Interpretations proposed so far have concentrated mostly on the S1 and S2 harmonic responses (Pinault & Baubron 1996; Richon *et al.* 2009; Crockett *et al.* 2010). When no S2 peak was observed in radon concentration time-series, for example, in Alpine grassland (Perrier

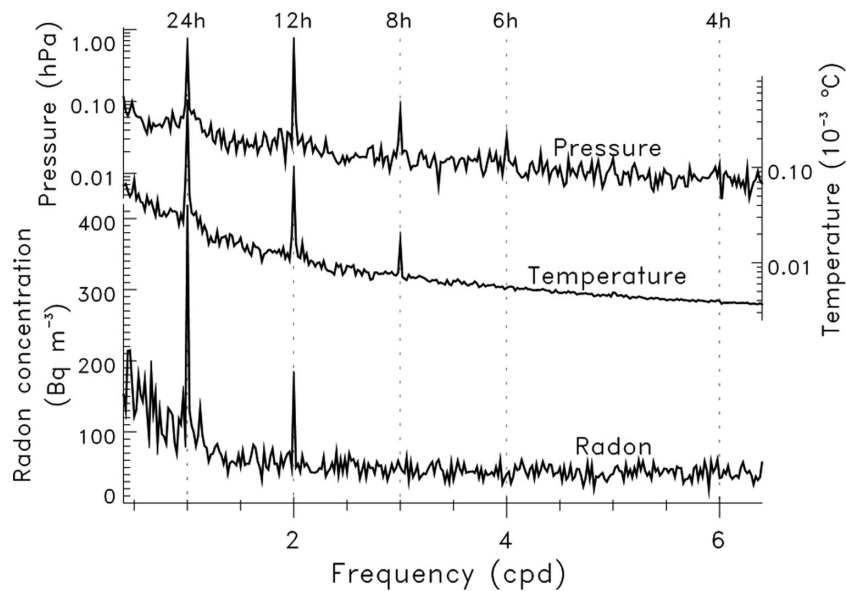


Figure 18. Amplitude spectra of radon concentration, temperature and atmospheric pressure recorded in 2005, with a sampling time of 1 hr, at a depth of 30 cm in the soil at the Syabru-Bensi hydrothermal system in Central Nepal (Perrier *et al.* 2009b).

et al. 2009a), it has been tempting to conclude that both soil and shallow bedrock were impermeable. In this case, this conclusion was actually confirmed by independent measurements and direct observation, but, by itself, an observation using radon alone was not sufficient. For example, we have exhibited configurations with high permeability giving a small S2 response in the shallow radon concentration (Table 1), including the simple situation of the homogeneous half-space (case 3, Fig. 4).

When a S2 response appears in the radon time-series, interpretation also needs to remain cautious. Let us consider, for example, a time-series of radon concentration obtained at 30 cm depth in the soil near the Syabru-Bensi hot springs in Central Nepal (Perrier *et al.* 2009b; Crockett *et al.* 2010; Richon *et al.* 2011). An amplitude spectrum is shown in Fig. 18, together with the amplitude spectra of temperature and atmospheric pressure recorded at the same location with the same sensor (a BMC2 probe from Alcade, France). At the latitude of Nepal (28°N), the barometric tide S2 is conspicuous (1.2 hPa), but the S1 amplitude is also large (1 hPa). In the radon amplitude spectrum, the dominating response is a diurnal wave, with amplitude about 800 Bq m⁻³, with a significant S2 peak with amplitude 400 Bq m⁻³. Both the S1 and S2 responses of radon concentration show contrasted seasonal variations (Richon *et al.* 2011), with the S1 response being large during the wet summer season and the S2 response being large during the dry winter season.

Our calculations can shed some lights on these observations, taking in this case $P_0 = 860$ hPa. First, we do not expect a large difference of response at 24 hr and at 12 hr, thus the fact that the S1 and S2 peaks in the radon spectrum are different, while the amplitudes of the barometric oscillations are similar, indicates that most of the S1 radon response must be due to a different effect, and, most likely, a soil temperature effect. Since the S2 peaks show up during the dry season while the S1 variation is small, the S2 peak must be due to atmospheric pressure only, with little contamination from higher harmonics of temperature variations. This is also suggested by the fact that no significant S3 peak is observed in the radon signal. The fact that no higher harmonics of S2 is observed at 4 or 6 cpd in the amplitude spectrum of radon concentration is reasonable. We have shown (Fig. 10) that the higher harmonics are attenuated rapidly with increasing order, except in unusual circumstances (case 5), which seem to be excluded on this particular site. The observed S2 amplitude (400 Bq m⁻³) is rather significant, while not exceptional, among our studied cases (Table 1). This suggests that an interface with contrasted values of EC_{Ra} must be present in the near-vicinity of the probe to sustain such a large S2 amplitude. No S2 response is observed when the radon probes are installed at 1 m depth (Richon *et al.* 2011), suggesting that a possible heterogeneity must be located between 1 m and 30 cm depth, a hypothesis that can be checked on site.

6 CONCLUSION AND PERSPECTIVES

In this paper, we present a complete analytical calculation of the harmonic response of radon flux and concentration to a surface oscillation of atmospheric pressure, in the case of a bedrock covered by a soil layer. The response is dramatically affected by the presence of an interface and interpretations using simplified models based on a homogeneous half-space can be misleading. In general, the conditions leading to large harmonic response are non-trivial and the large response is often localized in the immediate vicinity of the interface, and therefore easy to miss in a blind experiment. Another result, important in practice for hydrothermal systems, is the fact that, when advection is large, then harmonic response is damped at all orders in radon concentration, except, possibly, the fundamental harmonic of the surface radon flux. In addition to grasping the physical complexity of the response, our analytical calculations, also, can be useful when testing numerical models (Ferry *et al.* 2002; Rinaldi *et al.* 2012).

Further refinements could be considered, and some are listed in the following with increasing importance. Other parametrizations of the radon diffusion coefficient (Meslin *et al.* 2010) could be tested, as well as other more elaborated expressions for the relative permeability (Van Genuchten 1980; Ferry *et al.* 2002). Furthermore, the effects of anisotropy and dispersion (Auer *et al.* 1996; Massman 2006) might need to be considered. Nevertheless, such developments are meaningful only after detailed comparisons with experimental data are available. At this time, indeed, the harmonic response of radon to barometric oscillation in the shallow soil, while mentioned in some studies (Richon *et al.* 2009, 2011), has not been studied in sufficient details since the initial pioneering studies (Pinault & Baubron 1996). One important question that will need to be addressed with experimental data is whether the boundary conditions are valid in the immediate vicinity of the surface, or need to be modified as suggested by some authors (Antonopoulos-Domis *et al.* 2009).

Beyond single harmonic oscillations, such as the S2 wave, the first and higher orders transfer functions between atmospheric pressure and radon concentration might also be studied versus frequency, so that radon flux and concentration time-series can be calculated. This problem is fundamentally different from the precise calculation of the effect of a given oscillation, as we have developed in this study, but is of tremendous interest, especially for the estimation of the net flux excess (enhancement factor) induced in average by the presence of barometric pumping. One important hypothesis in our calculation is the assumption of a steady state. Whether a steady state really can exist in the soil, always exposed to numerous external factors, is an open problem, which probably cannot be ignored in the future when studying barometric pumping of any component, including radon.

At some sites, such as active volcanoes (Zimmer & Erzinger 2003; Cigolini *et al.* 2009), the approach developed in this paper might be largely insufficient, as temperature effects are considered to play an important role in shaping the response to pressure variations. Before dedicated models are developed, nevertheless, it is necessary to investigate whether the observed response of radon is anomalous and incompatible with the predictions of a simple soil over bedrock configuration. Our results indicate, indeed, that the response can show surprising features in particular regions of the parameter space.

While currently available time-series might be revisited in light of our theoretical results, dedicated experiments need to be considered so that large responses to barometric oscillations can be observed and analysed. To search for large S2 in order to estimate permeability, it is necessary, first, to study carefully the static radon distribution, so that the sensors can be installed at the locations of the largest gradients. For the moment, few studies address the static spatial distribution of radon in the vicinity of the probes installed for long-term measurements. It would be helpful to choose a site with a permeable soil over permeable bedrock, close to the conditions covered by the calculations. Once the static radon distribution is established, ideally to a depth of at least 2 m, it would be useful to install sensors, including in the top part of the bedrock below the soil/bedrock interface, which is possible using probes installed in vertical pipes (Richon *et al.* 2011). When possible, measurements of radon concentration in the soil should be complemented by continuous measurements of radon flux at the surface (Ferry *et al.* 2001). When continuous radon flux measurements are not available, continuous measurements of CO₂ flux (Viveiros *et al.* 2008; Rinaldi *et al.* 2012) can provide complementary information. Ideally, it would be better to have time-series of both surface radon and CO₂ fluxes. Given the fact that seasonal effects are important and that, in particular, temperature effects complicate the interpretation, time-series of at least 2 yr duration would be necessary for a meaningful study.

More generally, experiments designed for other purposes, such as the monitoring of volcanoes or active faults, should be implemented in such a way that the basic physics and transport effects in the shallow layers, which still remain insufficiently well understood, could be studied in a comprehensive manner. While detailed studies might not be possible in all circumstances, the search for anomalous signals associated with geodynamical effects would benefit greatly if such detailed investigations could be carried out at least at selected locations. Actually, not only the harmonic response to barometric oscillations need to be studied, but the whole transfer function between radon parameters and atmospheric pressure, for frequencies between 10⁻⁷ and 10⁻³ Hz, would be of interest, with possible applications to transient signals analysis (Ferry *et al.* 2002). Barometric oscillations are also important to study in relation to Earth tide waves, such as M2 and O1 oscillations, for example, evidenced in radon concentration in a glacier cavity (Richon *et al.* 2012). This comparison provides an assessment of the sensitivity of a given site to crustal hydromechanical influences versus meteorological influences. Such a global assessment of forcing parameters is already undertaken by comparing S2 response to S1 response in the case of CO₂ flux monitoring of volcanic areas (Rinaldi *et al.* 2012). Recently, long-term radon monitoring in tectonically active areas has given clear indications of barometric oscillations (Kamra *et al.* 2013; Zafirir *et al.* 2013). Oscillations due to ambient temperature or possibly novel physical effects have also been documented in radon signals (Steinitz *et al.* 2011) or other observations (Sturrock *et al.* 2012). In radon time-series, the response to the barometric tide S2 appears certainly as one important ingredient in the still poorly known physics of transport in our environment.

ACKNOWLEDGEMENTS

The authors thank Gauthier Hulot and Edouard Kaminski from Institut de Physique du Globe de Paris for continuous and faithful support over the years. Olivier Sirol is warmly thanked for his magical talent in getting the computers and the software running. Enlightening discussions are acknowledged with Robin Crockett on the physics and data analysis of harmonic signals. The manuscript has been significantly improved thanks to the enlightened comments of several reviewers and the extremely careful work of the Editor. This paper is IGP contribution number 3416.

REFERENCES

- Al-Zoughool, M. & Krewski, D., 2009. Health effects of radon: a review of the literature, *Int. J. Radiat. Biol.*, **85**, 57–69.
- Antonopoulos-Domis, M., Xanthos, S., Clouvas, A. & Alifrangis, D., 2009. Experimental and theoretical study of radon distribution in soil, *Health Phys.*, **97**, 322–331.
- Auer, L.H., Rosenberg, N.D., Birdsell, K.H. & Whitney, E.M., 1996. The effects of barometric pumping on contaminant transport, *J. Contamin. Hydrol.*, **24**, 145–166.
- Barbosa, S.M., Steinitz, G., Piatibratova, O., Silva, M.E. & Lago, P., 2007. Radon variability at the Elat granite, Israel: heteroscedasticity and non-linearity, *Geophys. Res. Lett.*, **34**, L15309, doi:10.1029/2007GL030065.
- Barbosa, S.M., Zafrir, H., Malik, U. & Piatibratova, O., 2010. Multiyear to daily radon variability from continuous monitoring at the Amram tunnel, southern Israel, *Geophys. J. Int.*, **182**, 829–842.
- Baykara, O., Doğru, M., Inceöz, M. & Aksoy, E., 2005. Measurements of radon emanation from soil samples in triple-junction of North and East Anatolian active faults systems in Turkey, *Radiat. Meas.*, **39**, 209–212.
- Carslaw, H.S. & Jaeger, J.C., 1946. *Conduction of Heat in Solids*, Oxford University Press, 510 pp.
- Choubey, V.M., Arora, B.R., Barbosa, S.M., Kumar, N. & Kamra, L., 2011. Seasonal and daily variation of radon at 10 m depth in borehole, Garhwal Lesser Himalaya, India, *Appl. Radiat. Isot.*, **69**, 1070–1078.
- Cigolini, C. *et al.*, 2009. Radon surveys and real-time monitoring at Stromboli volcano: influence of soil temperature, atmospheric pressure and tidal forces on ^{222}Rn degassing, *J. Volcanol. Geotherm. Res.*, **184**, 381–388.
- Clements, W.E. & Wilkening, M.H., 1974. Atmospheric pressure effects on ^{222}Rn transport across the earth-air atmosphere, *J. Geophys. Res.*, **79**, 5025–5029.
- Crockett, R.G.M., Gillmore, G.K., Phillips, P.S., Denman, A.R. & Groves-Kirkby, C.J., 2006. Radon anomalies preceding earthquakes which occurred in the UK, in summer and autumn 2002, *Sci. Total Environ.*, **364**, 138–148.
- Crockett, R.G.M., Perrier, F. & Richon, P., 2010. Spectral-decomposition techniques for the identification of periodic and anomalous phenomena in radon time-series, *Nat. Hazards Earth Syst. Sci.*, **10**, 559–564.
- Darby, S. *et al.*, 2004. Radon in homes and risk of lung cancer: collaborative analysis of individual data from 13 European case-control studies, *Br. Med. J.*, **330**, 223–228.
- Eff-Darwich, A., Martín-Luis, C., Quesada, M., de la Nuez, J. & Coello, J., 2002. Variations on the concentration of ^{222}Rn in the subsurface of the volcanic island of Tenerife, Canary Islands, *Geophys. Res. Lett.*, **29**, 26-1–26-4.
- Ferry, C., Beneto, A., Richon, P. & Robé, M.C., 2001. An automatic device for measuring the effect of meteorological factors on radon-222 flux from soils in the long term, *Radiat. Prot. Dosim.*, **93**, 271–274.
- Ferry, C., Richon, P., Beneto, A. & Robé, M.C., 2002. Evaluation of the effect of a cover layer on radon exhalation from uranium mill tailings: transient radon flux analysis, *J. Environ. Radioact.*, **63**, 49–64.
- Fujiyoshi, R., Sakamoto, K., Imanishi, T., Sumiyoshi, T., Sawamura, S., Vaupotič, J. & Kobal, I., 2006. Meteorological parameters contributing to the variability in ^{222}Rn activity concentrations in soil gas at a site in Sapporo, Japan, *Sci. Total Environ.*, **370**, 224–234.
- Gillmore, G.K., Crockett, R.G.M. & Przylibski, T.A., 2010. IGCP Project 571: radon, health and natural hazards, *Nat. Hazards Earth Syst. Sci.*, **10**, 2051–2054.
- Girault, F. & Perrier, F., 2011. Heterogeneous temperature sensitivity of effective radium concentration with various rock and soil samples, *Nat. Hazards Earth Syst. Sci.*, **11**, 1619–1626.
- Girault, F. & Perrier, F., 2012a. Estimating the importance of factors influencing the radon-222 flux from building walls, *Sci. Total Environ.*, **433**, 247–263.
- Girault, F. & Perrier, F., 2012b. Measuring effective radium concentration with large numbers of samples. Part 2—general properties and representativity, *J. Environ. Radioact.*, **113**, 189–202.
- Girault, F., Gajurel, A.P., Perrier, F., Upreti, B.N. & Richon, P., 2011. Radon emanation of heterogeneous basin deposits in Kathmandu Valley, Nepal, *J. Asian Earth Sci.*, **40**, 595–610.
- Girault, F., Koirala, B.P., Perrier, F., Richon, P. & Rajaure, S., 2009. Persistence of radon-222 flux during monsoon at a geothermal zone in Nepal, *J. Environ. Radioact.*, **100**, 955–964.
- Groves-Kirkby, C.J., Denman, A.R., Crockett, R.G.M., Phillips, P.S. & Gillmore, G.K., 2006. Identification of tidal and climatic influences within domestic radon time-series from Northamptonshire, UK, *Sci. Total Environ.*, **367**, 191–202.
- Gutiérrez, J.L., García-Talavera, M., Peña, V., Nalda, J.C., Voytchev, M. & López, R., 2004. Radon emanation measurements using silicon photodiode detectors, *Appl. Radiat. Isot.*, **60**, 583–587.
- Ho, C.K., 2008. Analytical risk-based model of gaseous and liquid-phase radon transport in landfills with radium sources, *Environ. Modelling Softw.*, **23**, 1163–1170.
- Holford, D.J., Schery, S.D., Wilson, J.L. & Phillips, F.M., 1993. Modeling radon transport in dry, cracked soil, *J. geophys. Res.*, **98**, 567–580.
- Kämpf, H., Bräuer, K., Schumann, J., Hahne, K. & Strauch, G., 2013. CO_2 discharge in an active, non-volcanic continental rift area (Czech Republic): characterisation ($\delta^{13}\text{C}$, $^3\text{He}/^4\text{He}$) and quantification of diffuse and vent CO_2 emissions, *Chem. Geol.*, **339**, 71–83.
- Kamra, L., Choubey, V.M., Kumar, N., Rawat, G. & Khandelwal, D.D., 2013. Radon variability in borehole from Multi-Parametric Geophysical Observatory of NW Himalaya in relation to meteorological parameters, *Appl. Radiat. Isot.*, **72**, 137–144.
- Kitto, M.E., 2005. Interrelationship of indoor radon concentrations, soil-gas flux, and meteorological parameters, *J. Radioanal. Nucl. Chem.*, **264**, 381–385.
- Laiolo, M., Cigolini, C., Coppola, D. & Piscopo, D., 2012. Developments in real-time radon monitoring at Stromboli volcano, *J. Environ. Radioact.*, **105**, 21–29.
- Lee, K.Y., Yoon, Y.Y. & Ko, K.S., 2010. Determination of the emanation coefficient and the Henry's law constant for the groundwater radon, *J. Radioanal. Nucl. Chem.*, **286**, 381–385.
- Lehmann, B.E., Lehmann, M., Neftel, A. & Tarakanov, S.V., 2000. Radon-222 monitoring of soil diffusivity, *Geophys. Res. Lett.*, **27**, 3917–3920.
- Lewicki, J.L., Oldenburg, C.M., Dobeck, L. & Spangler, L., 2007. Surface CO_2 leakage during two shallow subsurface CO_2 releases, *Geophys. Res. Lett.*, **34**, L24402, doi:10.1029/2007GL032047.
- Lindzen, R.S. & Chapman, S., 1969. Atmospheric tides, *Space Sci. Rev.*, **10**, 3–188.
- Massmann, J. & Farrier, D.F., 1992. Effects of atmospheric pressures on gas transport in the vadose zone, *Water Res. Res.*, **28**, 777–791.
- Massman, W.J., 2006. Advective transport of CO_2 in permeable media induced by atmospheric pressure fluctuations: 1, an analytical model, *J. geophys. Res.*, **111**, G03004, doi:10.1029/2006JG000163.
- Meslin, P.-Y., Adler, P.M. & Sabroux, J.-C., 2010. Diffusive transport of gases in wet porous media. Application to radon, *Soil Sci. Soc. Am. J.*, **74**, 1871–1885.
- Nazaroff, W.W., 1992. Radon transport from soil to air, *Rev. Geophys.*, **30**, 137–160.
- Neeper, D.A., 2002. Investigation of the vadose zone using barometric pressure cycles, *J. Contamin. Hydrol.*, **54**, 59–80.
- Neeper, D.A. & Stauffer, P., 2005. Unidirectional gas flow in soil porosity resulting from barometric pressure cycles, *J. Contamin. Hydrol.*, **78**, 281–289.
- Neri, M., Behncke, B., Burton, M., Galli, G., Giammanco, S., Pecora, E., Privitera, E. & Reitano, D., 2006. Continuous soil radon monitoring during the July 2006 Etna eruption, *Geophys. Res. Lett.*, **33**, L24316, doi:10.1029/2006GL028394.
- Nguyen, D.C., Chruściel, E. & Prokólski, Ł., 2005. Factors controlling measurements of radon mass exhalation rate, *J. Environ. Radioact.*, **82**, 363–369.
- Nilson, R.H., Peterson, E.W., Lie, K.H., Burkhard, N.R. & Hearst, J.R., 1991. Atmospheric pumping: a mechanism causing vertical transport of contaminated gases through fractured permeable media, *J. geophys. Res.*, **96**, 21 933–21 948.

- Owczarski, P.C., Holford, D.J., Freeman, H.D. & Gee, G.W., 1990. Effects of changing water content and atmospheric pressure on radon flux from surfaces of five soil types, *Geophys. Res. Lett.*, **17**, 817–820.
- Papastefanou, C., 2002. An overview of instrumentation for measuring radon in soil gas and groundwaters, *J. Environ. Radioact.*, **63**, 271–283.
- Perrier, F. & Richon, P., 2010. Spatiotemporal variation of radon and carbon dioxide concentrations in an underground quarry: coupled processes of natural ventilation, barometric pumping and internal mixing, *J. Environ. Radioact.*, **101**, 279–296.
- Perrier, F., Richon, P. & Sabroux, J.-C., 2009a. Temporal variations of radon concentration in the saturated soil of Alpine grassland: the role of groundwater flow, *Sci. Total Environ.*, **407**, 2361–2371.
- Perrier, F., Richon, P., Crouzeix, C., Morat, P. & Le Mouél, J.-L., 2004. Radon-222 signatures of natural ventilation regimes in an underground quarry, *J. Environ. Radioact.*, **71**, 17–32.
- Perrier, F. *et al.*, 2009b. A direct evidence for high carbon dioxide and radon-222 discharge in Central Nepal, *Earth planet. Sci. Lett.*, **278**, 198–207.
- Pinault, J.-L. & Baubron, J.-C., 1996. Signal processing of soil gas radon, atmospheric pressure, moisture, and soil temperature data: a new approach for radon concentration modeling, *J. geophys. Res.*, **101**, 3157–3171.
- Pohl-Rüling, J. & Pohl, E., 1969. The radon-222 concentration in the atmospheres of mines as a function of the barometric pressure, *Health Phys.*, **16**, 579–584.
- Porstendörfer, J., 1994. Properties and behaviour of radon and thoron and their decay products in the air, *J. Aerosol Sci.*, **25**, 219–263.
- Richon, P., Perrier, F., Pili, E. & Sabroux, J.-C., 2009. Detectability and significance of 12 hr barometric tide in radon-222 signal, dripwater flow rate, air temperature and carbon dioxide concentration in an underground tunnel, *Geophys. J. Int.*, **176**, 683–694.
- Richon, P., Moreau, L., Sabroux, J.-C., Pili, E. & Salaün, A., 2012. Evidence of both M₂ and O₁ Earth tide waves in radon-222 air concentration in a subglacial laboratory, *J. geophys. Res.*, **117**, B12404, doi:10.1029/2011JB009111.
- Richon, P., Perrier, F., Koirala, B.P., Girault, F., Bhattarai, M. & Sapkota, S.N., 2011. Temporal signatures of advective versus diffusive radon transport at a geothermal zone in Central Nepal, *J. Environ. Radioact.*, **102**, 88–102.
- Richon, P., Sabroux, J.-C., Halbwachs, M., Vandemeulebrouck, J., Poussielgue, N., Tabbagh, J. & Punongbayan, R., 2003. Radon anomaly in the soil of Taal volcano, the Philippines: a likely precursor of the M7.1 Mindoro earthquake (1994), *Geophys. Res. Lett.*, **30**, 1481, doi:10.1029/2003GL016902.
- Richon, P., Bernard, P., Labed, V., Sabroux, J.-C., Beneito, A., Lucius, D., Abbad, S. & Robé, M.-C., 2007. Results of monitoring ²²²Rn in soil gas of the Gulf of Corinth region, Greece, *Radiat. Meas.*, **42**, 87–93.
- Riley, W.J., Gadgil, A.J., Bonnefous, Y.C. & Nazaroff, W.W., 1996. The effect of steady winds on radon-222 entry from soil into houses, *Atmos. Environ.*, **30**, 1167–1176.
- Riley, W.J., Robinson, A.L., Gadgil, A.J. & Nazaroff, W.W., 1999. Effects of variable wind speed and direction on radon transport from soil into buildings: model development and exploratory results, *Atmos. Environ.*, **33**, 2157–2168.
- Rinaldi, A.P., Vandemeulebrouck, J., Todesco, M. & Viveiros, F., 2012. Effects of atmospheric conditions on surface diffuse degassing, *J. geophys. Res.*, **117**, B11201, doi:10.1029/2012JB009490.
- Robinson, A.L., Sextro, R.G. & Riley, W.J., 1997. Soil-gas entry into houses driven by atmospheric pressure fluctuations—the influence of soil properties, *Atmos. Environ.*, **31**, 1487–1495.
- Rogers, V.C. & Nielson, K.K., 1991a. Correlations for predicting air permeabilities and ²²²Rn diffusion coefficients of soils, *Health Phys.*, **61**, 225–230.
- Rogers, V.C. & Nielson, K.K., 1991b. Multiphase radon generation and transport in porous materials, *Health Phys.*, **60**, 807–815.
- Sakoda, A., Hanamoto, K., Ishimori, Y., Nagamatsu, T. & Yamaoka, K., 2008. Radioactivity and radon emanation fraction of the granites sampled at Misasa and Badgastein, *Appl. Radiat. Isot.*, **66**, 648–652.
- Sakoda, A., Ishimori, Y., Hanamoto, K., Kataoka, T., Kawabe, A. & Yamaoka, K., 2010. Experimental and modeling studies of grain size and moisture content effects on radon emanation, *Radiat. Meas.*, **45**, 204–210.
- Sakoda, A., Ishimori, Y. & Yamaoka, K., 2011. A comprehensive review of radon emanation measurements for mineral, rock, soil, mill tailing and fly ash, *Appl. Radiat. Isot.*, **69**, 1422–1435.
- Schery, S.D. & Gaeddert, D.H., 1982. Measurements of the effect of cyclic atmospheric pressure variation on the flux of ²²²Rn from the soil, *Geophys. Res. Lett.*, **9**, 835–838.
- Schery, S.D., Gaeddert, D.H. & Wilkening, M.H., 1984. Factors affecting exhalation of radon from a gravelly sandy loam, *J. geophys. Res.*, **89**, 7299–7309.
- Simpson, G.C., 1919. The twelve-hourly barometer oscillation, *Q. J. R. Meteorol. Soc.*, **44**, 1–18.
- Steinitz, G. & Piatibratova, O., 2010. Radon signals in the Gavnunim intrusion, Makhtesh Ramon, Israel, *Geophys. J. Int.*, **180**, 651–665.
- Steinitz, G., Piatibratova, O. & Barbosa, S.M., 2007. Radon daily signals in the Elat Granite, southern Arava, Israel, *J. geophys. Res.*, **112**, B10211, doi:10.1029/2006JB004817.
- Steinitz, G., Piatibratova, O. & Kotlarsky, P., 2011. Possible effect of solar tides on radon signals, *J. Environ. Radioact.*, **102**, 749–765.
- Stoulos, S., Manolopoulou, M. & Papastefanou, C., 2003. Assessment of natural radiation exposure and radon exhalation from building materials in Greece, *J. Environ. Radioact.*, **69**, 225–240.
- Stranden, E., Kolstad, A.K. & Lind, B., 1984. The influence of moisture and temperature on radon exhalation, *Radiat. Prot. Dosim.*, **7**, 55–58.
- Sturrock, P.A., Steinitz, G., Fischbach, E., Javorek, D. II & Jenkins, J.H., 2012. Analysis of gamma radiation from a radon source: indications of a solar influence, *Astropart. Phys.*, **36**, 18–25.
- Sundal, A.V., Valen, V., Soldal, O. & Strand, T., 2008. The influence of meteorological parameters on soil radon levels in permeable glacial sediments, *Sci. Total Environ.*, **389**, 418–428.
- Tanner, A.B., 1964. Radon migration in the ground: a review, in *The Natural Radiation Environment*, pp. 161–190, eds Adams, J.A.S. & Lowder, W.M., University of Chicago Press.
- Van Genuchten, M.T., 1980. A closed-form equation for predicting the hydraulic conductivity of unsaturated soils, *Soil Sci. Soc. Am. J.*, **44**, 892–898.
- Viñas, R., Eff-Darwich, A., Soler, V., Martín-Luis, M.C., Quesada, M.L. & de la Nuez, J., 2007. Processing of radon time series in underground environments: implications for volcanic surveillance in the island of Tenerife, Canary Islands, Spain, *Radiat. Meas.*, **42**, 101–115.
- Viveiros, F., Ferreira, T., Cabral Vieira, J., Silva, C. & Gaspar, J.L., 2008. Environmental influences on soil CO₂ degassing at Furnas and Fogo volcanoes (São Miguel Island, Azores archipelago), *J. Volcanol. Geotherm. Res.*, **177**, 883–893.
- Viveiros, F., Cardellini, C., Ferreira, T., Caliro, S., Chiodini, G. & Silva, C., 2010. Soil CO₂ emissions at Furnas volcano, São Miguel Island, Azores archipelago: volcano monitoring perspectives, geomorphologic studies, and land use planning application, *J. geophys. Res.*, **115**, B12208, doi:10.1029/2010JB007555.
- Washington, J.W. & Rose, A.W., 1992. Temporal variability of radon concentration in the interstitial gas of soils in Pennsylvania, *J. geophys. Res.*, **97**, 9145–9159.
- White, G.J. & Rood, A.S., 2001. Radon emanation from NORM contaminated pipe scale and soil at petroleum industry sites, *J. Environ. Radioact.*, **54**, 401–413.
- Zafir, H., Barbosa, S.M. & Malik, U., 2013. Differentiation between the effect of temperature and pressure on radon within the subsurface geological media, *Radiat. Meas.*, **49**, 39–56.
- Zimmer, M. & Erzinger, J., 2003. Continuous H₂O, CO₂, ²²²Rn and temperature measurements on Merapi volcano, Indonesia, *J. Volcanol. Geotherm. Res.*, **125**, 25–38.

APPENDIX A: EXPLICIT SOLUTION FOR CONSTANTS OF THE HARMONIC EXPANSION IN THE ADVECTIVE-DIFFUSIVE CASE

A1 Solution for $n = 0$

The three constants B_{20} , B_{10} and \tilde{B}_{10} satisfy the following equations (see Section 2.3.2):

$$\left\{ \begin{array}{l} c_{10}(0) = c_e \\ c_{10}(z_1) = c_{20}(z_1) \\ \varepsilon_1^g D_1^g \left. \frac{dc_{10}}{dz} \right|_{z=z_1} = \varepsilon_2^g D_2^g \left. \frac{dc_{20}}{dz} \right|_{z=z_1} \end{array} \right. , \tag{A1}$$

which, using eq. (24), can be rewritten:

$$\left\{ \begin{array}{l} \hat{c}_1 + B_{10} + \tilde{B}_{10} = c_e \\ \hat{c}_1 + B_{10}b_{10} + \tilde{B}_{10}\tilde{b}_{10} = \hat{c}_2 + B_{20}b_{20} \\ B_{10}b_{10}\beta_{10}^+ + \tilde{B}_{10}\tilde{b}_{10}\beta_{10}^- = RB_{20}b_{20}\beta_{20}^+ \end{array} \right. , \tag{A2}$$

with

$$b_{j0} = e^{\beta_{j0}^+ z_1}, \quad \tilde{b}_{j0} = e^{\beta_{j0}^- z_1} \quad \text{and} \quad R = \frac{\varepsilon_2^g D_2^g}{\varepsilon_1^g D_1^g}. \tag{A3}$$

Straightforward manipulation of eq. (A2) then leads to:

$$B_{10} = \frac{(c_e - \hat{c}_1)(R\beta_{20}^+ - \beta_{10}^-) + (\hat{c}_1 - \hat{c}_2) \frac{R\beta_{20}^+}{\tilde{b}_{10}}}{R\beta_{20}^+ - \beta_{10}^- + \frac{b_{10}}{\tilde{b}_{10}}(\beta_{10}^+ - R\beta_{20}^+)}, \tag{A4}$$

$$\tilde{B}_{10} = \frac{(c_e - \hat{c}_1)(\beta_{10}^+ - R\beta_{20}^+) - (\hat{c}_1 - \hat{c}_2) \frac{R\beta_{20}^+}{b_{10}}}{\frac{\tilde{b}_{10}}{b_{10}}(R\beta_{20}^+ - \beta_{10}^-) + \beta_{10}^+ - R\beta_{20}^+} \tag{A5}$$

and

$$B_{20} = \frac{(c_e - \hat{c}_1)(\beta_{10}^+ - \beta_{10}^-) + (\hat{c}_2 - \hat{c}_1) \left(\frac{\beta_{10}^-}{b_{10}} - \frac{\beta_{10}^+}{\tilde{b}_{10}} \right)}{\frac{b_{20}}{b_{10}}(R\beta_{20}^+ - \beta_{10}^-) + \frac{b_{20}}{\tilde{b}_{10}}(\beta_{10}^+ - R\beta_{20}^+)}. \tag{A6}$$

A2 Solution for $n \geq 1$

To determine the constants B_{2n} , B_{1n} and \tilde{B}_{1n} , $n \geq 1$, we first have the condition $c_{jn}(z = 0) = 0$, which, using eq. (39), reads:

$$\sum_{k=0}^{M_n-3} C_{1k}^n + B_{1n} + \tilde{B}_{1n} = 0. \tag{A7}$$

At $z = z_1$, the separate continuity of each harmonic term n of the concentration, using eq. (16), gives:

$$c_{1n}(z_1)e^{n\gamma_1(1+i)z_1} = c_{2n}(z_1)e^{n\gamma_2(1+i)z_1}, \tag{A8}$$

which reads:

$$\sum_{k=0}^{M_n-3} C_{1k}^n e^{n\gamma_1^k z_1} + B_{1n}b_{1n} + \tilde{B}_{1n}\tilde{b}_{1n} = \chi_n \left(\sum_{k=0}^{M_n-3} C_{2k}^n e^{n\gamma_2^k z_1} + B_{2n}b_{2n} \right), \tag{A9}$$

with

$$b_{jn} = e^{\beta_{jn}^+ z_1}, \quad \tilde{b}_{jn} = e^{\beta_{jn}^- z_1} \tag{A10}$$

and

$$\chi_n = e^{n(\gamma_2 - \gamma_1)(1+i)z_1}. \tag{A11}$$

For the radon flux, the flow and the concentration being continuous in eq. (6), the continuity of each harmonic term n of the flux containing the first derivative of the concentration gives:

$$\varepsilon_1^g D_1^g \left(\left. \frac{dc_{1n}}{dz} \right|_{z=z_1} + c_{1n}(z_1)n\gamma_1(1+i) \right) e^{n\gamma_1(1+i)z_1} = \varepsilon_2^g D_2^g \left(\left. \frac{dc_{2n}}{dz} \right|_{z=z_1} + c_{2n}(z_1)n\gamma_2(1+i) \right) e^{n\gamma_2(1+i)z_1}, \tag{A12}$$

which reads:

$$\begin{aligned} & \sum_{k=0}^{M_n-3} C_{1k}^n (\eta_{1k}^n + n\gamma_1(1+i)) e^{\eta_{1k}^n z_1} + B_{1n} (\beta_{1n}^+ + n\gamma_1(1+i)) b_{1n} + \tilde{B}_{1n} (\beta_{1n}^- + n\gamma_1(1+i)) \tilde{b}_{1n} \\ &= R\chi_n \left(\sum_{k=0}^{M_n-3} C_{2k}^n (\eta_{2k}^n + n\gamma_2(1+i)) e^{\eta_{2k}^n z_1} + B_{2n} (\beta_{2n}^+ + n\gamma_2(1+i)) b_{2n} \right). \end{aligned} \tag{A13}$$

Let us define the following sums of previously known quantities:

$$\Gamma_0^n = \sum_{k=0}^{M_n-3} C_{1k}^n, \tag{A14}$$

$$\Gamma_1^n = \sum_{k=0}^{M_n-3} C_{1k}^n e^{\eta_{1k}^n z_1}, \tag{A15}$$

$$\Gamma_2^n = \chi_n \sum_{k=0}^{M_n-3} C_{2k}^n e^{\eta_{2k}^n z_1}, \tag{A16}$$

$$\tilde{\Gamma}_1^n = \sum_{k=0}^{M_n-3} C_{1k}^n (\eta_{1k}^n + n\gamma_1(1+i)) e^{\eta_{1k}^n z_1}, \tag{A17}$$

$$\tilde{\Gamma}_2^n = \chi_n \sum_{k=0}^{M_n-3} C_{2k}^n (\eta_{2k}^n + n\gamma_2(1+i)) e^{\eta_{2k}^n z_1} \tag{A18}$$

and

$$v_{jn}^\pm = \beta_{jn}^\pm + n\gamma_j(1+i). \tag{A19}$$

Then, continuity eqs (A7), (A9) and (A13) lead to the following system of equations:

$$\begin{cases} B_{1n} + \tilde{B}_{1n} = -\Gamma_0^n \\ B_{1n} b_{1n} + \tilde{B}_{1n} \tilde{b}_{1n} = \Gamma_2^n - \Gamma_1^n + B_{2n} b_{2n} \chi_n \\ B_{1n} b_{1n} v_{1n}^+ + \tilde{B}_{1n} \tilde{b}_{1n} v_{1n}^- = R\tilde{\Gamma}_2^n - \tilde{\Gamma}_1^n + R B_{2n} b_{2n} \chi_n v_{2n}^+ \end{cases} \tag{A20}$$

Straightforward manipulation of eq. (A20) then leads to the following explicit solutions for the remaining constants at order n :

$$B_{1n} = \frac{-\Gamma_0^n (Rv_{2n}^+ - v_{1n}^-) - (\Gamma_2^n - \Gamma_1^n) \frac{Rv_{2n}^+}{\tilde{b}_{1n}} + (R\tilde{\Gamma}_2^n - \tilde{\Gamma}_1^n) \frac{1}{\tilde{b}_{1n}}}{Rv_{2n}^+ - v_{1n}^- + \frac{b_{1n}}{\tilde{b}_{1n}} (v_{1n}^+ - Rv_{2n}^+)}, \tag{A21}$$

$$\tilde{B}_{1n} = \frac{-\Gamma_0^n (v_{1n}^+ - Rv_{2n}^+) + (\Gamma_2^n - \Gamma_1^n) \frac{Rv_{2n}^+}{b_{1n}} - (R\tilde{\Gamma}_2^n - \tilde{\Gamma}_1^n) \frac{1}{b_{1n}}}{\frac{\tilde{b}_{1n}}{b_{1n}} (Rv_{2n}^+ - v_{1n}^-) + v_{1n}^+ - Rv_{2n}^+} \tag{A22}$$

and

$$B_{2n} = \frac{-\Gamma_0^n (v_{1n}^+ - v_{1n}^-) + (\Gamma_2^n - \Gamma_1^n) \left(\frac{v_{1n}^-}{b_{1n}} - \frac{v_{1n}^+}{\tilde{b}_{1n}} \right) - (R\tilde{\Gamma}_2^n - \tilde{\Gamma}_1^n) \left(\frac{1}{b_{1n}} - \frac{1}{\tilde{b}_{1n}} \right)}{\frac{b_{2n}\chi_n}{b_{1n}} (Rv_{2n}^+ - v_{1n}^-) + \frac{b_{2n}\chi_n}{\tilde{b}_{1n}} (v_{1n}^+ - Rv_{2n}^+)}. \tag{A23}$$

APPENDIX B: ANALYTICAL TREATMENT IN THE PURELY ADVECTIVE CASE

When the diffusion term is neglected, eqs (21) and (28) become:

$$-W_{j0} \frac{d\bar{c}_{j0}}{dz} - \lambda \bar{c}_{j0} = -\lambda \hat{c}_j, \tag{B1}$$

and

$$-\bar{X}_{jn} \frac{d\bar{c}_{jn}}{dz} - \bar{Y}_{jn} \bar{c}_{jn} = -s_j(1+i)(A_j - B_j e^{-2\gamma_j(1+i)z}) \left(\frac{d\bar{c}_{j(n-1)}}{dz} + (n-1)\gamma_j(1+i)\bar{c}_{j(n-1)} \right), \tag{B2}$$

for $n \geq 1$, with:

$$\begin{cases} \bar{X}_{jn} = W_{j0} \\ \bar{Y}_{jn} = \lambda + ni\omega + W_{j0}n\gamma_j(1+i) \end{cases}, \tag{B3}$$

for $n \geq 0$.

The general solution of the left-hand side of the differential equation in eq. (B2) is of the form $\bar{c}_{jn}(z) = e^{-\bar{\beta}_{jn}z}$ with:

$$\bar{\beta}_{jn} = \frac{\bar{Y}_{jn}}{\bar{X}_{jn}} = \frac{\lambda + ni\omega}{W_{j0}} + n\gamma_j(1+i). \tag{B4}$$

Let us first consider the static solution ($n = 0$). The solution for medium j can be written:

$$\bar{c}_{j0}(z) = \hat{c}_j + \bar{C}_{j0}^0 e^{-\bar{\beta}_{j0}z}. \tag{B5}$$

Since the real part of $\bar{\beta}_{j0}$ is positive, a finite solution for $z = -\infty$ requires $\bar{C}_{(N-1)0}^0 = 0$. The constants for the other layers can be found by iteration. Indeed, continuity of the concentration at each interface for $0 \leq j \leq N - 2$ imposes:

$$\bar{c}_{(j+1)0}(z_j) = \bar{c}_{j0}(z_j), \tag{B6}$$

which, using eq. (B5), leads to the following iterative relation:

$$\bar{C}_{j0}^0 = e^{\bar{\beta}_{j0}z_j} \left(\hat{c}_{j+1} - \hat{c}_j + \bar{C}_{(j+1)0}^0 e^{-\bar{\beta}_{(j+1)0}z_j} \right). \tag{B7}$$

For the n harmonics, $n \geq 1$, following the method developed previously, we write the solution $\bar{c}_{jn}(z)$ as a sum of \bar{M}_n exponential terms:

$$\bar{c}_{jn}(z) = \sum_{k=0}^{\bar{M}_n-1} \bar{C}_{jk}^n e^{\bar{\eta}_{jk}^n z}, \tag{B8}$$

and we know already $\bar{M}_0 = 1$ and $\bar{\eta}_{j0}^0 = -\bar{\beta}_{j0}$. Now, we can express iteratively the constants for harmonic n as a function of constants for harmonic $n - 1$, which provides a complete solution.

The right-hand side of eq. (B2) becomes:

$$-s_j(1+i)(A_j - B_j e^{-2\gamma_j(1+i)z}) \sum_{k=0}^{\bar{M}_{n-1}-1} \bar{C}_{jk}^{n-1} (\bar{\eta}_{jk}^{n-1} + (n-1)\gamma_j(1+i)) e^{\bar{\eta}_{jk}^{n-1} z}, \tag{B9}$$

hence a sum of $2\bar{M}_{n-1}$ exponential terms.

A particular solution of eq. (B2) can be exhibited in the form:

$$\sum_{k=0}^{2\bar{M}_{n-1}-1} \bar{C}_{jk}^n e^{\bar{\eta}_{jk}^n z}, \tag{B10}$$

with, for $0 \leq k \leq \bar{M}_{n-1} - 1$, the following parameters:

$$\bar{\eta}_{jk}^n = \bar{\eta}_{jk}^{n-1}, \tag{B11}$$

$$\bar{C}_{jk}^n = -s_j(1+i)A_j \frac{\bar{\eta}_{jk}^{n-1} + (n-1)\gamma_j(1+i)}{-\bar{X}_{jn}\bar{\eta}_{jk}^n - \bar{Y}_{jn}} \bar{C}_{jk}^{n-1} \tag{B12}$$

and, for $\bar{M}_{n-1} \leq k \leq 2\bar{M}_{n-1} - 1$:

$$\bar{\eta}_{jk}^n = \bar{\eta}_{jk}^{n-1} - 2\gamma_j(1+i), \tag{B13}$$

$$\bar{C}_{jk}^n = s_j(1+i)B_j \frac{\bar{\eta}_{jk}^{n-1} + (n-1)\gamma_j(1+i)}{-\bar{X}_{jn}\bar{\eta}_{jk}^n - \bar{Y}_{jn}} \bar{C}_{jk}^{n-1}. \tag{B14}$$

The general solution of eq. (B2) then is the sum of the general solution of the left-hand side of eq. (B2), namely $e^{-\tilde{\beta}_j n z}$, as given above, and the particular solution given by eq. (B10):

$$\bar{c}_{jn}(z) = \sum_{k=0}^{2\tilde{M}_{n-1}-1} \bar{C}_{jk}^n e^{\tilde{\beta}_{jk}^n z} + \bar{C}_{j(\tilde{M}_{n-1})}^n e^{-\tilde{\beta}_j n z}, \tag{B15}$$

which is of the form given by eq. (B8) with:

$$\tilde{M}_n = 2\tilde{M}_{n-1} + 1, \tag{B16}$$

$$\tilde{\eta}_{j(\tilde{M}_{n-1})}^n = -\tilde{\beta}_j n. \tag{B17}$$

According to eq. (B16), for $n = 1$, the solution is a sum of 3 exponential terms, for $n = 2$, a sum of 7 terms, for $n = 3$, a sum of 15 terms, and for $n = 4$, a sum of 31 terms. The expression of the constants $\bar{C}_{j(\tilde{M}_{n-1})}^n$ can be found by imposing the boundary condition that for layer $N - 1$ the harmonic term n for $n \geq 1$ is 0:

$$\bar{c}_{(N-1)n}(z \leq z_{N-2}) = 0. \tag{B18}$$

Continuity of the harmonic n of concentration at each interface then reads for $0 \leq j \leq N - 2$:

$$\bar{c}_{jn}(z_j) e^{n\gamma_j(1+i)z_j} = \bar{c}_{(j+1)n}(z_j) e^{n\gamma_{j+1}(1+i)z_j}, \tag{B19}$$

which, using eq. (B8), gives the following iterative expression:

$$\bar{C}_{j(\tilde{M}_{n-1})}^n = e^{\tilde{\beta}_j n z_j} \left(\bar{c}_{(j+1)n}(z_j) e^{n(\gamma_{j+1}-\gamma_j)(1+i)z_j} - \sum_{k=0}^{\tilde{M}_n-2} \bar{C}_{jk}^n e^{\tilde{\beta}_{jk}^n z_j} \right). \tag{B20}$$

In this case, the concentration at the surface is no longer constrained by the surface boundary conditions, but is imposed by the system. This is mathematically expressed by the fact that the constants are now sufficiently well constrained without an additional condition at the surface. Furthermore, physically, in the case of strong advection, it is not possible to maintain a static concentration equal to c_e and to have zero harmonic terms with $n \geq 1$. The harmonic n of the concentration at surface can then be calculated as:

$$\bar{c}_{sn} = \bar{c}_{1n}(0) = \hat{c}_1 \delta_{n0} + \sum_{k=0}^{\tilde{M}_n-1} \bar{C}_{1k}^n, \tag{B21}$$

with $\delta_{ij} = 0$ when $i \neq j$ and $\delta_{ij} = 1$ when $i = j$, and the harmonic n of the flux at the surface Φ_{sn} is:

$$\begin{cases} \Phi_{s0} = V_0 \bar{c}_{s0} \\ \Phi_{sn \geq 1} = V_0 \bar{c}_{sn} - s_1 \varepsilon_1^g (1+i) (A_1 - B_1) \bar{c}_{s(n-1)} \end{cases} \tag{B22}$$

APPENDIX C: SUMMARY OF PHYSICAL QUANTITIES

Quantity	Symbol	Unit (value)
Radon-222 decay constant	λ	s^{-1} (2.1×10^{-6})
Radon-222 diffusion coefficient in air	D_0	$m^2 s^{-1}$ (1.2×10^{-5})
Radon-222 water to air concentration ratio	κ_w	
Soil temperature	T	$^{\circ}C$
Frequency	f	Hz
Pulsation (angular velocity)	ω	$rad s^{-1}$
Mean absolute atmospheric pressure	P_0	Pa
Surface atmospheric pressure excess	$p_s(t)$	Pa
Harmonic amplitude of atmospheric pressure	p_0	Pa
Dynamic viscosity of gas	η_g	Pa s (1.8×10^{-5})
Bottom of layer j	z_j	m
Depth	z	m
Mineral matrix density of layer j	ρ_j	$kg m^{-3}$
Porosity of layer j	ε_j	
Permeability of layer j	k_j	m^2
Permeability for water phase in layer j	k_j^w	m^2
Permeability for gaseous phase in layer j	k_j^g	m^2
Volumetric water saturation in layer j	S_{wj}	
Water-phase porosity in layer j	ε_j^w	

Quantity	Symbol	Unit (value)
Gaseous-phase porosity in layer j	ε_j^g	
Effective radium concentration in layer j	EC_{Raj}	Bq kg ⁻¹
Pressure variation at time t and depth z in layer j	$p_j(z, t)$	Pa
Specific vertical advective flow rate	V_0	m s ⁻¹
Gaseous-specific flow rate in layer j	$F_j(z, t)$	
Radon concentration in layer j	$c_j(z, t)$	Bq m ⁻³
Radon concentration in the open atmosphere	c_e	Bq m ⁻³
Radon flux at the surface	$\Phi_s(t)$	Bq m ⁻² s ⁻¹
Radon flux at position z in layer j	$\Phi_j(z, t)$	Bq m ⁻² s ⁻¹
Pneumatic diffusivity in layer j	α_j	m ² s ⁻¹
Inverse of pneumatic attenuation length in layer j	γ_j	m ⁻¹
Diffusion coefficient of radon in layer j	D_j^g	m ² s ⁻¹
Equilibrium radon concentration in layer j in the absence of air flow	\hat{c}_j	Bq m ⁻³
Term n in the harmonic expansion of $c_{jn}(z)$	$c_{jn}(z)$	Bq m ⁻³
Number of terms in the development of $c_{jn}(z)$	M_n	
Radon concentration in layer j in the purely diffusive case	$\bar{c}_j(z, t)$	Bq m ⁻³
Term n in the harmonic expansion of $\bar{c}_j(z, t)$	$\bar{c}_{jn}(z)$	Bq m ⁻³
Number of terms in the development of $\bar{c}_{jn}(z)$	\bar{M}_n	

SUPPORTING INFORMATION

Additional Supporting Information may be found in the online version of this article:

Figure S1. Harmonic 1 specific flow versus soil water saturation (a) and versus bedrock water saturation (b), at the ground surface and at two depth positions (30 and 65 cm). Fixed parameters correspond to case 1 in Table 1. Surface pressure oscillation is a S2 wave with 100 Pa amplitude.

Figure S2. Static and harmonic amplitudes of surface radon flux (a) and radon concentration at 45 cm depth (b) versus soil water saturation. Fixed conditions refer to case 1 in Table 1 and a S2 oscillation with 100 Pa amplitude.

Figure S3. Static and harmonic amplitudes of surface radon flux (a) and radon concentration at 45 cm depth (b) versus soil permeability. Fixed conditions refer to case 2 in Table 1 and a S2 oscillation with 100 Pa amplitude.

Figure S4. Static and harmonic amplitudes of surface radon flux (a) and radon concentration at 45 cm depth (b) versus ratio bedrock permeability to soil permeability. Fixed conditions refer to case 1 in Table 1 and a S2 oscillation with 100 Pa amplitude.

Figure S5. Static and harmonic amplitudes of surface radon flux (a) and radon concentration at 65 cm depth (b) versus soil porosity. Fixed conditions refer to case 2 in Table 1 and a S2 oscillation with 100 Pa amplitude.

Figure S6. Static and harmonic amplitudes of surface radon flux (a) and radon concentration at 65 cm depth (b) versus bedrock porosity. Fixed conditions refer to case 2 in Table 1 and a S2 oscillation with 100 Pa amplitude. (<http://gji.oxfordjournals.org/lookup/suppl/doi:10.1093/gji/ggt280/-/DC1>)

Please note: Oxford University Press are not responsible for the content or functionality of any supporting materials supplied by the authors. Any queries (other than missing material) should be directed to the corresponding author for the article.